An unprecedented combination of metabolic pathways in the cryptic plastid of a non-photosynthetic euglenophyte

Zoltán Füssy[1,2,#], Kristína Záhonová[1,2,3,#], Aleš Tomčala[1,§], Juraj Krajčovič[4], Vyacheslav Yurchenko[3], Miroslav Oborník[1,5], Marek Eliáš[3,*]

[1] Institute of Parasitology, Biology Centre ASCR, 370 05 České Budějovice, Czech Republic

[2] Faculty of Science, Charles University, BIOCEV, 252 50 Vestec, Czech Republic

[3] Life Science Research Centre, Department of Biology and Ecology and Institute of Environmental Technologies, Faculty of Science, University of Ostrava, 701 00 Ostrava, Czech Republic

[4] Department of Biology, Faculty of Natural Sciences, University of ss. Cyril and Methodius in Trnava, 917 01 Trnava, Slovakia

[5] University of South Bohemia, Faculty of Science, 370 05 České Budějovice, Czech Republic

[#] These authors contributed equally to this work.

[§] Present address: University of South Bohemia, Faculty of Fisheries and Protection of Waters, CENAKVA, 370 05 České Budějovice, Czech Republic

[*] Corresponding author:

E-mail: marek.elias@osu.cz (ME)

Abstract

The non-photosyntetic alga *Euglena longa* harbours a cryptic plastid of unknown function. By a combination of bioinformatic and biochemical approaches we found out that this organelle houses a surprising set of metabolic processes. Biosynthesis of isoprenoid precursors and fatty acids is absent and the tetrapyrrole pathway is incomplete, whereas phospholipids and glycolipids are still being produced in the *E. longa* plastid. Unprecedented among non-photosynthetic plastids is the ability of this organelle to make tocopherols and a phylloquinone derivative. The most striking attribute is the presence of a linearized Calvin-Benson (CB) pathway including RuBisCO, together with ferredoxin-$NADP^+$ reductase and the ferredoxin/thioredoxin system. We hypothesize that the linear CB pathway is regulated by the redox status of the *E. longa* cell, in effect functioning as a redox valve bypassing the glycolytic oxidation of glyceraldehyde-3-phosphate to 3-phosphoglycerate. Altogether, the *E. longa* plastid defines a new class of relic plastids.

Key words: Calvin-Benson cycle, Euglenophyceae, evolution, non-photosynthetic plastids, phylloquinone, redox balance

Abbreviations: ACP, acyl carrier protein; CBC, Calvin-Benson cycle; FAS, fatty acid synthesis; GAPDH, glyceraldehyde 3-phosphate dehydrogenase; IPP, isopentenyl pyrophosphate; MEP, 2-C-methyl-d-erythritol 4-phosphate; MGDG/DGDG mono-/digalactosyldiacylglycerol; MVA, mevalonate; OH-PhQ, 5'-monohydroxyphylloquinone; PhQ, phylloquinone; SQDG, sulfoquinovosyldiacylglycerol; SP, signal peptide; TMD, transmembrane domain

Introduction

Plastids are organelles that evolved from a cyanobacterial endosymbiont in the ancestor of Archaeplastida and later found their way into other eukaryotic lineages by secondary or even higher-order endosymbioses (Keeling 2013; McFadden 2014; Ponce-Toledo et al. 2017). Photosynthetic harvesting of solar energy is supposedly the primary metabolic function and evolutionary advantage of plastid acquisition. However, plastids also host a variety of other metabolic pathways, such as biosynthesis of amino and fatty acids, isopentenyl pyrophosphate (IPP) and its derivatives (isoprenoids), and tetrapyrroles (Neuhaus and Emes 2000; Oborník and Green 2005; Van Dingenen et al. 2016). Hence, reversion of photosynthetic lineages to heterotrophy typically does not imply plastid loss, and non-photosynthetic plastids are found in many eukaryotic lineages (Wilson et al. 1996; Sanchez-Puerta et al. 2007; Slamovits and Keeling 2008; Janouškovec et al. 2015; Kamikawa et al. 2017; Hadariová et al. 2018). In these cases, metabolic integration

of the plastid presumably resulted in the host biochemistry being dependent on compound(s) supplied by the organelle (Oborník et al. 2009; Lim and McFadden 2010; Janouškovec et al. 2015; Hadariová et al. 2018).

The most extensively studied relic plastid is undoubtedly the apicoplast of apicomplexan parasites (especially of *Plasmodium falciparum* and *Toxoplasma gondii*). The knowledge of the apicoplast has expanded tremendously since its discovery two decades ago (McFadden and Yeh 2017). The apicoplast is ultimately derived from a red alga (Williamson et al. 1994; Moore et al. 2008; Janouškovec et al. 2010), with an ochrophyte alga being a possible direct donor of the plastids in apicomplexans and their photosynthetic relatives, chromerids (Ševčíková et al. 2015; Füssy and Oborník 2017). Except for the recently characterized corallicolid apicomplexans (Kwong et al. 2019), the apicoplast genome contains only genes related to gene expression, protein turnover, and assembly of FeS clusters, not considering a few short hypothetical open reading frames of unknown function (Wilson et al. 1996; Janouškovec et al. 2015). The essentiality of the apicoplast for parasite survival has attracted much attention, partly because this organelle is a promising target for parasite-specific inhibitors (e.g. Miller et al. 2013; McFadden and Yeh 2017). So far, three plastid pathways (encoded by the nuclear genome) seem to condition the apicoplast retention: non-mevalonate IPP synthesis, haem synthesis, and type II fatty acid synthesis (FASII). IPP biosynthesis in particular is vital for the bloodstream form of *P. falciparum* (Yeh and DeRisi 2011). On the other hand, the mosquito and liver stages of *P. falciparum* are dependent on haem synthesis (Nagaraj et al. 2013), while FASII is indispensable for pellicle formation in *Toxoplasma gondii* (Ke et al. 2014; Martins-Duarte et al. 2016).

Less is known about the actual metabolic functions of plastids in other non-photosynthetic algal lineages. Many of them have a similar metabolic capacity as the apicoplast (Sanchez-Puerta et al. 2007; Slamovits and Keeling 2008; Fernández Robledo et al. 2011), and some house an even more complex metabolism that includes amino acid biosynthesis and carbohydrate metabolism pathways (Borza et al. 2005; Pombert et al. 2014; Smith and Lee 2014). Until recently, IPP synthesis seemed to be a process conserved even in the most reduced relic plastids, such as the genome-lacking plastids of certain alveolates (Matsuzaki et al. 2008; Janouškovec et al. 2015), but non-photosynthetic plastids lacking the characteristic plastidial (MEP or DOXP) pathway of IPP biosynthesis are now known (Kamikawa et al. 2017; Graupner et al. 2018; Dorrell et al. 2019). Thus, there is generally a metabolic reason for a plastid retention, although the cases of plastid dependency differ between lineages.

An interesting group to study non-photosynthetic plastids are the euglenophytes. Like their prime representative *Euglena gracilis*, most euglenophytes are mixotrophs containing a complex three-membranes-bound photosynthetic plastid derived from a green alga belonging to Pyramimonadales (Turmel et al. 2009; Leander et al. 2017; Jackson et al. 2018). However, non-photosynthetic mutants of *E. gracilis*,

induced by an antibiotic or mutagenic treatment, are often capable of heterotrophic living even after presumed plastid loss (reviewed in Krajčovič et al. 2002; Hadariová et al. 2018). This might be enabled by metabolic independence of the *E. gracilis* cell on the plastid. For instance, *E. gracilis* was shown to possess two parallel haem synthesis pathways, one located in the mitochondrion/cytosol and another in the plastid (Weinstein and Beale 1983). In the long run, this redundancy might predestine one of the pathways for loss, provided that the other can efficiently supply the end-product to all compartments requiring it (Kořený and Oborník 2011; Cihlář et al. 2016). On the other hand, localization of an essential pathway or its part exclusively into the plastid will impose essentiality of the organelle as such.

Several lineages of euglenophytes independently became secondarily heterotrophic, but evidence for the presence of a plastid has been provided only for *Euglena longa* (originally called *Astasia longa*), a close relative of *E. gracilis* (Marin et al. 2003; Nudelman et al. 2003). The documentation of the organelle at the cytological level is spurious (Webster et al. 1967; Kivic and Vesk 1974; Hachtel 1996), but the complete plastid genome sequence was reported nearly two decades ago (Gockel and Hachtel 2000). As expected, it lacks all the photosynthesis-related genes, except for *rbcL* encoding the large subunit of ribulose-1,5-bisphosphate carboxylase/oxygenase (RuBisCO). We recently documented the existence of a nucleus-encoded small subunit (RBCS) of the *E. longa* RuBisCO enzyme synthesized as a precursor polyprotein, but its processing into monomers could not be demonstrated (Záhonová et al. 2016). The physiological role of the *E. longa* RuBisCO and the whole plastid remains unknown, although indirect evidence suggests that the plastid is essential for *E. longa* survival (Siemeister et al. 1990a, b; Gockel et al. 1994; Hadariová et al. 2017).

To provide a key resource for investing the biology of *E. longa* and its plastid, we recently generated a transcriptome assembly for this species and demonstrated that it is complete and directly comparable to the transcriptome assemblies reported for *E. gracilis* (Záhonová et al. 2018). Evaluation of a set of high-confidence candidates for plastid-targeted proteins enabled us to conclude that nucleus-encoded plastidial proteins in *E. longa* employ N-terminal targeting presequences of the same two characteristic classes, as known from *E. gracilis*. The *E. longa* transcriptome revealed various unusual features of the plastid biogenesis and maintenance machinery shared with photosynthetic euglenophytes, but also supported the lack of the photosynthesis-related machinery and suggested specific reductions of several plastidial house-keeping functions presumably reflecting the loss of photosynthesis (Záhonová et al. 2018). However, the repertoire of anabolic and catabolic pathways localized to the *E. longa* colourless plastid has not been investigated and is the subject of the present paper.

To chart the main paths of the metabolic map of the *E. longa* plastids, we searched for homologs of enzymes underpinning pathways known from plastids of other species. The reconstruction was greatly facilitated by the recent characterization of the *E. gracilis* plastid metabolic network based on a proteomic

123 analysis of the organelle (Novák Vanclová et al. 2019). N-terminal regions of the candidates were evaluated
124 for characteristics of presequences predicting a specific subcellular localization to distinguish those likely
125 representing plastid-targeted proteins from enzymes located to other parts of the cell. Some of the
126 bioinformatics predictions were further tested by biochemical analyses. Our study provides the first
127 comprehensive view of a non-photosynthetic secondary plastid of green-algal origin and shows that the
128 metabolic capacity of the *E. longa* plastid is strikingly different from those of the apicoplast and other relic
129 plastids characterized in sufficient detail.
130
131
132 **Results and Discussion**
133 ***E. longa* plastid lacks the MEP pathway of IPP biosynthesis, yet has kept the production of tocopherol**
134 **and a phylloquinone derivative**
135 Two parallel pathways of IPP biosynthesis exist in *E. gracilis* (Kim et al. 2004): the mevalonate (MVA)
136 pathway localized to the mitochondrion (first three enzymes) and the cytosol (the rest), and the plastid-
137 localized 2-C-methyl-D-erythritol (MEP) pathway, but only enzymes of the MVA pathway were found in
138 *E. longa* (Table S1, Fig. 1A). *E. longa* thus joins the group of recently discovered plastid-bearing eukaryotes
139 lacking the MEP pathway, namely the colourless diatom *Nitzschia* sp. NIES-3581 (Kamikawa et al. 2017)
140 and various colourless chrysophytes (Graupner et al. 2018; Dorrell et al. 2019). In contrast, the plastid-
141 localized MEP pathway in apicomplexans and related alveolates (i.e. Myzozoa) is essential as a source of
142 precursors for the synthesis of all cellular isoprenoids, since the cytosolic MVA pathway was lost from this
143 group (Janouškovec et al. 2015; Waller et al. 2016). The retention of the MEP pathway in the colourless
144 plastids of diverse non-photosynthetic chlorophytes (Figueroa-Martinez et al. 2015) is similarly explained
145 by the loss of the MVA pathway in this group (Lohr et al. 2012).
146 The MEP pathway in *E. gracilis* provides precursors for the synthesis in the plastid of terpenoid
147 compounds connected to photosynthesis, namely carotenoids and plastoquinone (Kim et al. 2004; Novák
148 Vanclová et al. 2019). As expected, the respective enzymes are all missing from *E. longa*. However, we
149 were surprized to find out that the *E. longa* plastid appears still involved in terpenoid metabolism,
150 specifically in its phytol branch. Photosynthetic eukaryotes generally produce three types of phytol
151 derivatives, tocopherols (vitamin E), phylloquinone (PhQ; vitamin K_1) and chlorophyll (its phytyl chain),
152 starting with a common precursor phytyl-PP, which is (directly or indirectly via salvage of phytol liberated
153 by chlorophyll degradation) made by reduction of geranylgeranyl-PP synthesized in the plastid by the MEP
154 pathway (Gutbrod et al. 2019). *E. gracilis* proved to be unusual not only because of lacking the conventional
155 geranylgeranyl-PP reductase (Novák Vanclová et al. 2019), but also for making phytol from precursors
156 provided by the MVA pathway (Disch et al. 1998; Kim et al. 2004). The route of phytol synthesis from the

157 cytosolic isoprenoids is currently unknown, though it was proposed that phytyl-PP is synthesized in the *E.*
158 *gracilis* plastid exclusively by step-wise phosphorylation of phytol by phytol kinase (VTE5) and phytyl
159 phosphate kinase (VTE6), which are enzymes normally employed for recycling phytol from chlorophyll
160 degradation (Novák Vanclová et al. 2019). This scheme is supported by the fact that *E. longa* has retained
161 VTE5 as well as VTE6, both proteins being highly similar to their *E. gracilis* orthologs and exhibiting
162 putative plastid targeting presequences (Fig. S1; Table S1). Since *E. longa* lacks chlorophyll, these two
163 enzymes must have a function independent of phytol recycling.
164 In addition of its role in chlorophyll synthesis, phytyl-PP is used by *E. gracilis* to make tocopherols
165 and a PhQ derivative, 5'-monohydroxyphylloquinone (OH-PhQ; Ziegler et al. 1989; Watanabe et al. 2017;
166 Novák Vanclová et al. 2019). All four enzymes mediating synthesis of α-tocopherol from phytyl-PP and
167 homogentisate were identified in *E. gracilis* and are localized to its plastid (Novák Vanclová et al. 2019).
168 Interestingly, orthologs of all four enzymes are found in *E. longa* as well, all with a typical plastid-targeting
169 presequence or at least with the N-terminal region being highly similar to the *E. gracilis* counterpart (Table
170 S1), consistent with their presumed plastidial localization (Fig. 1A). Homogentisate itself is apparently made
171 outside the plastid, most likely in the mitochondrion, as the enzyme responsible for its synthesis (4-
172 hydroxyphenylpyruvate dioxygenase) is not found in the *E. gracilis* plastid proteome and the respective
173 proteins have a predicted mitochondrial transit peptide in both *E. gracilis* and *E. longa* (Table S1). Our
174 analysis thus predicts that like its photosynthetic cousin, *E. longa* produces α-tocopherol. To test this
175 directly, we analysed extracts from *E. longa* by means of HPLC-MS/MS. For comparison, we employed
176 samples from *E. gracilis* grown at two different conditions (in light and in darkness). Tocopherols were
177 detected in both species (Fig. 1B), with α-tocopherol being the dominant form present in equivalent amounts
178 in all three samples (Fig. 1C). The signals of β- and/or γ-tocopherol (indistinguishable by our method) and
179 of δ-tocopherol suggest that tocopherol cyclase, and possibly also tocopherol O-methyltransferase, of both
180 *Euglena* species can process substrates with or without the 3-methyl group on the benzene ring (Fig. S2).
181 The synthesis of OH-PhQ in *E. gracilis* is understood only partially, with only three enzymes of the
182 pathway previously identified at the molecular level: the large multifunctional protein PHYLLO, apparently
183 localized to the cytosol and catalysing the first four steps leading to o-succinylbenzoate; MenA catalysing
184 phytylation of dihydroxynaphthoate localized in the plastid; and MenG (demethylnaphthoquinone
185 methyltransferase), possessing a typical N-terminal plastid-targeting presequence but not directly confirmed
186 as plastidial by proteomics (Novák Vanclová et al. 2019). Strikingly, *E. longa* expresses homologs of these
187 three *E. gracilis* proteins, although at low levels resulting in a low RNA-seq read coverage and thus
188 incomplete or inaccurate assembly of two of the respective transcripts (the PHYLLO sequence split into
189 several contigs, the MenA sequence with a frameshift corrected by RT-PCR; see Materials and Methods).
190 Nevertheless, N-terminal parts of both sequences were intact and confirmed the same subcellular

191 localization as in *E. gracilis* (Fig. 1A, Table S1). In agreement with these insights, OH-PhQ could be
192 detected in an extract from the *E. longa* culture (Fig. 1D, Fig. S3), although its abundance was smaller
193 compared to that in *E. gracilis* by an order of magnitude (Fig. 1E).

194 These findings document another unexpected function of the *E. longa* plastid, OH-PhQ synthesis,
195 albeit the plastid-associated part of the pathway cannot be presently reconstructed in full detail. One
196 uncertainty concerns the middle steps of the pathway, since like *E. gracilis* (see Novák Vanclová et al.
197 2019), *E. longa* also lack homologs of the conventional enzymes that are responsible for converting *o*-
198 succinylbenzoate to dihydroxynaphthoate and localized (at least in eukaryotes studied in sufficient detail)
199 in the peroxisome (Cenci et al. 2018). In contrast, tentative evidence was presented for the association of
200 the respective enzyme activities (presumably corresponding to enzymes non-orthologous to the
201 conventional ones) with the plastid envelope in *E. gracilis* (Seeger and Bentley 1991), raising a possibility
202 of a similar arrangement in *E. longa*. Secondly, the molecular identity of the putative hydroxylase catalysing
203 the final step of OH-PhQ synthesis is unknown, so its plastidial localization in *E. gracilis* or *E. longa* cannot
204 be ascertained. It is, nevertheless, likely given the fact that OH-PhQ is primarily needed in the plastid, at
205 least in photosynthetic eukaryotes (Ziegler et al. 1989). Thirdly, a previously unknown step – reduction of
206 the naphthoquinone ring – was recently demonstrated as a prerequisite for the reaction catalysed by MenG
207 to proceed in plants and cyanobacteria (Fatihi et al. 2015). The respective reductase is well conserved among
208 diverse plant and algal groups as well as cyanobacteria (Cenci et al. 2018), but we did not identify its close
209 homologs in any of the euglenophytes transcriptome assemblies, suggesting that euglenophytes employ an
210 alternative enzyme that yet needs to be characterized.

211 *E. longa* seems to be the first eukaryote with a non-photosynthetic plastid documented to have
212 retained the pathways (or final parts thereof) for tocopherols and OH-PhQ synthesis localized in the
213 organelle. The presence of tocopherols in *E. longa* is, however, not that surprising, as their function is not
214 restricted to photosynthetic tissues in plants and were detected also in bleached (i.e. non-photosynthetic) *E.*
215 *gracilis* mutants (Maeda and DellaPenna 2007; Watanabe et al. 2017). As potent lipophilic antioxidants
216 involved especially in membrane protection from damage caused by lipid peroxidation, tocopherols might
217 be used by *E. longa* as part of its protective mechanisms against reactive oxygen species generated by the
218 action of mitochondria and peroxisomes. The retention of OH-PhQ synthesis in *E. longa* may seem more
219 puzzling, given the fact that the best-established role of (OH-)PhQ in plants and algae is its functioning as
220 an electron carrier within the photosystem I (Ziegler et al. 1989; Brettel 1997). PhQ was additionally
221 proposed to serve as an electron acceptor in the process of disulfide bond formation in thylakoid lumenal
222 proteins required for proper function of photosystem II (Furt et al. 2010; Karamoko et al. 2011). A homolog
223 of the respective oxidoreductase (LTO1) exists in *E. gracilis* (Table S1), but not in the transcriptome data
224 from *E. longa*, consistent with the lack of photosystem II, and perhaps thylakoids entirely in the latter

225 species. Interestingly, PhQ was detected in the plasma membrane in plant tissues and proposed to be
226 involved in photosynthesis-unrelated redox processes at the cell surface (Lochner et al. 2003; Schopfer et
227 al. 2008). PhQ may even be synthesised directly in the plasma membrane, as a recent report from plants has
228 documented the existence of alternative forms of the terminal enzymes of PhQ biosynthesis that result from
229 alternative splicing and are localized to the plasma membrane rather than the plastid (Gu et al. 2018).
230 However, the protein sequences of both MenA and MenG enzymes in *E. longa* carry typical plastid-targeting
231 presequences, so they are unlikely to operate in the plasma membrane. We thus propose that OH-PhQ in *E.*
232 *longa* is involved in a hitherto uncharacterized, photosynthesis-unrelated plastid-resident process.
233

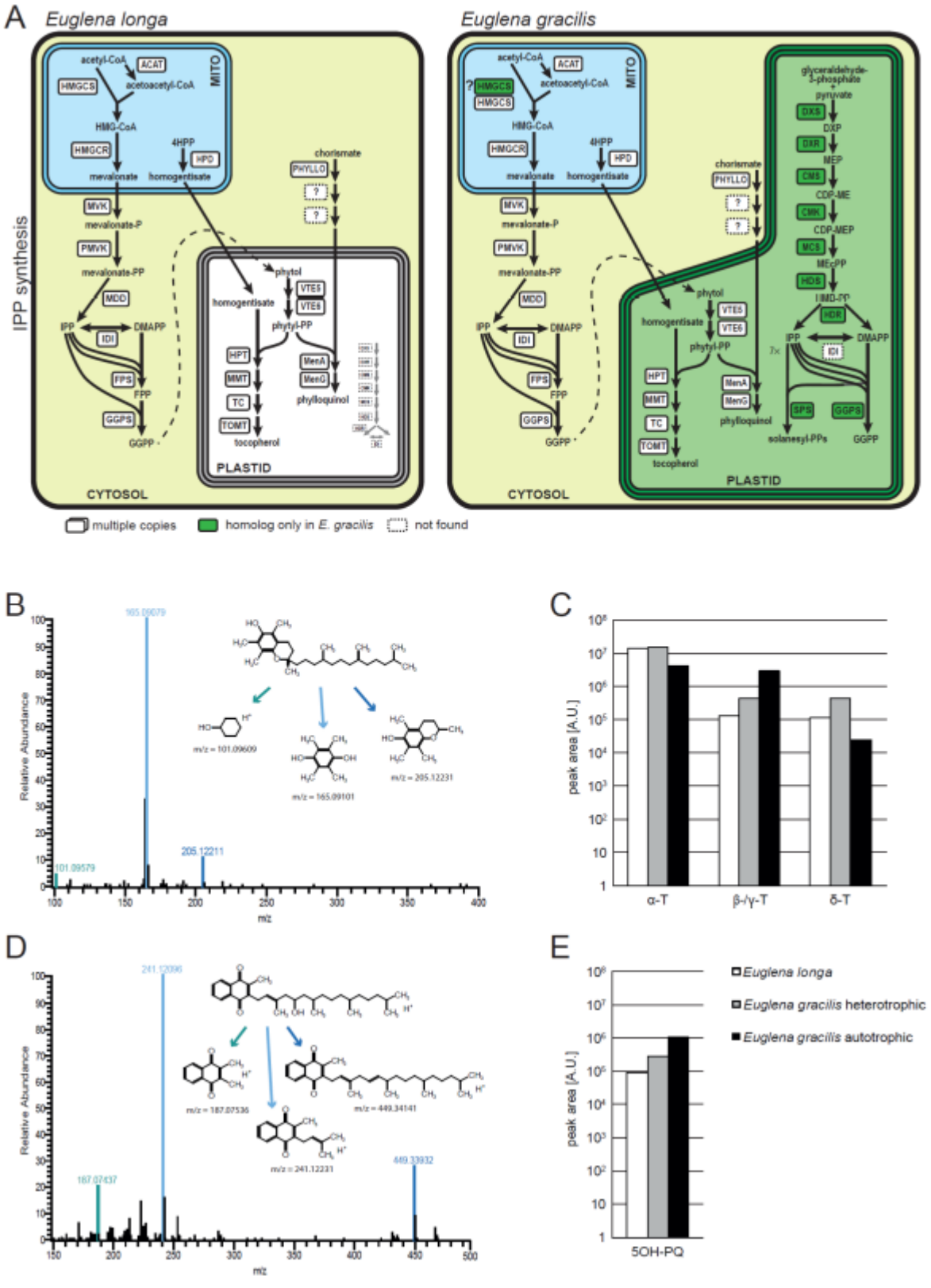

Figure 1: IPP and terpenoid-quinone biosynthesis in *E. longa* and its phototrophic relative *E. gracilis*.

A: Schematic comparison of the localization and evolutionary origin of enzymes (see colour-coding graphical legend below the "cells"). Abbreviations, IPP synthesis: ACAT – acetyl-CoA acetyltransferase, CDP-ME – 4-(cytidine 5'-diphospho)-2-C-methyl-D-erythritol, CDP-MEP – 2-phospho-CDP-ME, CMK – CDP-ME kinase, CMS – CDP-ME synthase, DMAPP – dimethylallyl diphosphate, DXP – 1-deoxy-D-xylulose 5-phosphate, DXR – DXP reductase, DXS – DXP synthase, FPP – farnesyl siphosphate synthase, GGPS – geranylgeranyl-diphosphate synthase, HDR – HMB-PP reductase, HDS – HMB-PP synthase, HMB-PP – 4-hydroxy-3-methylbut-2-en-1-yl diphosphate, HMG-CoA – 3-hydroxy-3-methylglutaryl-CoA, HMGCR – HMG-CoA reductase, HMGCS – HMG-CoA synthase, IDI – isopentenyl-diphosphate delta-isomerase, MCS – MEcPP synthase, MDD – mevalonate-diphosphate decarboxylase, MEcPP – 2-C-methyl-D-erythritol 2,4-cyclodiphosphate, MEP – 2-C-methyl-D-erythritol 4-phosphate, MVK – mevalonate kinase, PMVK – phosphomevalonate kinase, PPS – unspecified polyprenyl-diphosphate synthase, ? – unclear substrate; Terpenoid-quinone synthesis: 4HPP – 4-hydroxyphenylpyruvate, HPD – hydroxyphenylpyruvate dioxygenase, HPT – homogentisate phytyltransferase, MMT – MPBQ/MPSQ methyltransferase, TAT – tyrosine aminotransferase, TC – tocopherol cyclase, TMT – tocopherol-O-methyltransferase, VTE5 – phytyl kinase, VTE6 – phytyl-phosphate kinase. **B:** MS/MS spectrum record of *E. longa* α-tocopherol and the proposed fragmentation pattern in positive ionization mode (inset). Monoisotopic masses of particular fragments were obtained by simulation in Xcalibur software. **C:** Semiquantitative comparison of tocopherol species in *E. longa*, heterotrophically (dark) grown *E. gracilis* and autotrophic *E. gracilis*. **D and E:** MS/MS spectrum record of *E. longa* 5-hydroxyphylloquinone and the proposed fragmentation pattern in positive ionization mode (inset); semiquantitative comparison of 5-hydroxyphylloquinone.

E. longa plastid plays a limited role in the metabolism of nitrogen-containing compounds

Some of the apparent oddities of the *E. longa* plastid do not stem from the loss of photosynthesis in this species but reflect unusual features of the plastid in euglenophytes in general. These particularly concern plastid functions in the metabolism of nitrogen-containing compounds. Plastid is commonly involved in nitrogen assimilation due to housing nitrite reductase (Giordano and Raven 2014; Sanz-Luque et al. 2015), but it was established a long time ago that *E. gracilis* cannot assimilate nitrate or nitrite (Oda et al. 1979; Kitaoka et al. 1989) and, accordingly, no nitrite reductase can be identified in the transcriptome data from this species and *E. longa*. The plastids of both *Euglena* species apparently also lack the enzymes working immediately downstream, i.e. glutamine synthetase and glutamine oxoglutarate aminotransferase (the GS/GOGAT system common in plastids of other groups; Fernandez and Galvan 2008; Dagenais-Bellefeuille and Morse 2013), indicating that the plastids rely on the import of organic nitrogen from other parts of the cell, like recently proposed for the plastid in chromerids (Füssy et al. 2019).

One of the most surprising insights of the recent proteomics-aided analysis of the *E. gracilis* plastid metabolism was the paucity of pathways concerning amino acids (Novák Vanclová et al. 2019). *E. longa* is apparently even more extreme in this regard, because it lacks counterparts of the (predicted or proteomically verified) plastid-targeted forms of serine biosynthesis enzymes found previously in *E. gracilis*, i.e. phosphoglycerate dehydrogenase and phosphoserine phosphatase. Thus, we could localize only two elements of amino acid biosynthesis pathways to the *E. longa* plastid (Fig. S4): serine/glycine hydroxymethyltransferase, whose obvious role is to provide the one-carbon moiety for formylmethionyl-tRNA synthesis required for the plastidial translation; and one of the multiple isoforms of cysteine synthase A, which (like in *E. gracilis*) apparently relies on O-acetyl-L-serine synthesized outside the plastid, due to the absence of a discernible plastid-localized serine O-acetyltransferase (see Novák Vanclová et al. 2019, and Table S2). This is not due to a general reduction of amino acid metabolism in *E. longa* or the incompleteness of the sequence data, as its transcriptome assembly includes homologs of enzymes required for the synthesis of all 20 proteinogenic amino acids, but the respective proteins have predicted localization in compartments other than the plastid (Table S2).

Amino acids in the plastid are not only substrates of protein synthesis, but also serve as precursors or nitrogen donors for the synthesis of various other compounds (Moffatt and Ashihara 2002; Gerdes et al. 2012). One such pathway, described in detail in the subsequent section, leads to tetrapyrroles. In contrast, the spectrum of reactions related to the metabolism of other nitrogen-containing cofactors or their precursors (B vitamins) is very limited in the plastids of both *Euglena* species. We identified only one such candidate in *E. longa* – the reaction of vitamin B6 salvage catalysed by pyridoxamine 5'-phosphate oxidase, whereas *E. gracilis* additionally expresses two plastid-targeted isoforms of pyridoxine 4-dehydrogenase (Table S3). *De novo* synthesis or salvage of purines and pyrimidines is also absent from the plastid of both *Euglena* species, except for one step present in *E. gracilis* but apparently not *E. longa*: the former exhibits two forms of CTP synthase, one presumably cytosolic and another with a plastid-targeting presequence and found in the plastid proteome reported by Novák Vanclová et al. 2019, whereas *E. longa* expresses an ortholog of only the cytosolic version (Table S3). The lack of a separate plastidial CTP source in *E. longa* may reflect the presumably lower magnitude of RNA synthesis (and possibly also less extensive phospholipid synthesis requiring CTP in the reaction catalysed by CDP-diacylglycerol pyrophosphatase) in its plastid. Finally, *E. longa* possesses an ortholog of an enzyme involved in the synthesis of polyamines (spermidine synthase) found in the plastid proteome of *E. gracilis* (Novák Vanclová et al. 2019), but (in contrast to the *E. gracilis* protein) its N-terminus does not fit the characteristics of a plastid-targeting presequence, suggesting that its subcellular localization may be outside of the plastid (Fig. S4). However, we found out that both *E. longa* and *E. gracilis* have another version of this enzyme with an obvious plastid-targeting-like presequence in both species (Table S3), so we cannot rule out the possibility that polyamines are produced in the *E. longa*

plastid after all.

A residual tetrapyrrole biosynthesis pathway of unclear function is retained in the *E. longa* plastid

Most plastid-bearing eukaryotes synthesize protoporphyrin IX, the common precursor of haem and chlorophyll, via a single pathway wholly or mostly localized to the plastid (Oborník and Green 2005; Cihlář et al. 2016; Füssy and Oborník 2017). *E. gracilis* is one of the known exceptions, because it possesses two independent protoporphyrin synthesis pathways, a mitochondrial-cytosolic and a plastid one (Fig. 2A; Weinstein and Beale 1983; Kořený and Oborník 2011; Lakey and Triemer 2016). Whereas all enzymes of the plastid pathway were identified at the sequence level, previous studies left some gaps in the enzyme assignment to the different steps of the mitochondrial-cytosolic pathway (Kořený and Oborník 2011; Lakey and Triemer 2016). The new sequence data from *E. gracilis* has now enabled us to identify all three missing enzymes of the mitochondrial-cytosolic pathway; specifically novel, apparently cytosolic, isoforms of uroporphyrinogen-III synthase (UROS) and uroporphyrinogen decarboxylase (UROD), and two variants of oxygen-independent coproporphyrinogen oxidase (CPOXi), one cytosolic and one perhaps localized to the mitochondrion. In addition, we found a third UROS homolog that carries a plastid-targeting presequence and constitutes a divergent sister group to the previously known euglenophyte plastidial UROS isoform (Fig. S5; Table S4). Indeed, it was detected in the experimentally determined plastid proteome, together with the previously known plastidial UROS isoform (protein IDs 16898 and 15143 in Novák Vanclová et al. 2019), but the functional significance of the plastidial UROS duplication remains unclear.

Our transcriptome data from *E. longa* revealed orthologs of all *E. gracilis* enzymes of the mitochondrial-cytosolic pathway with the same predicted subcellular localization, barring a single enzyme with an incomplete N-terminal sequence precluding confident prediction (Fig. 2A; Table S4). In contrast, orthologs of only six of the *E. gracilis* plastid-targeted enzymes could be identified in the transcriptome of *E. longa*: aminolevulinic acid dehydratase (ALAD), the two UROS isoforms, one of the UROD isoforms, one isoform of CPOXi, and protoporphyrinogen oxidase (PPOX). The first three proteins have putative plastid-targeting presequences, much like their *E. gracilis* orthologs. However, the respective CPOXi protein has a strong mitochondrial targeting presequence, whereas the UROD protein is devoid of any presequence and the presequence of the PPOX protein is markedly shorter and lacks the characteristics of a plastid-targeting signal (Fig. 2B; Table S4). This suggests that only ALAD and the two UROS isoforms are targeted to the plastid in *E. longa*, whereas the other enzymes have been retargeted to the cytosol or mitochondrion in the evolution of the *E. longa* lineage. Strikingly, a putative *E. longa* homolog of the *E. gracilis* plastid-localized porphobilinogen deaminase (PBGD), an enzyme for the reaction between those catalysed by ALAD and UROS, was previously detected at both the RNA (by a Northern blot) and protein level (by an immunoblot; Shashidhara and Smith 1991), but we could not identify the respective transcript

in the *E. longa* transcriptome data even when the raw reads were searched.

Intact isolated *E. gracilis* plastids are capable of chlorophyll synthesis from externally supplied 5-aminolevulinic acid (ALA; Gomez-Silva et al. 1985), so it is possible that the *E. longa* plastid can analogously import ALA from the cytoplasm, thus providing a substrate for the plastid-localized ALAD isoform (Fig. 2A). The surprising absence of the previously documented plastid-localized PBGD in our transcriptome data may be potentially accounted for by the lack of expression of the respective enzyme at culture conditions employed by us. Hence, the pathway may theoretically proceed up to uroporphyrinogen III (the product of the UROS enzyme) in the *E. longa* plastid, but the absence of enzymes for further processing of this compound towards haem and/or chlorophyll (consistent with the lack of photosystems and the cytochrome b_6f complex) indicates that it is consumed by another process.

Uroporphyrinogen III is indeed at the beginning of a separate branch converting it in three steps to sirohaem (Dailey et al. 2017), which serves as a cofactor of several enzymes, including nitrite reductase and sulfite reductase (Tripathy et al. 2010). The former enzyme is missing from the *Euglena* spp. (see above), but sulfite reductase is present in both *E. longa* and *E. gracilis* (Table S4) and was detected in the plastid proteome of the latter species (Novák Vanclová et al. 2019). Hence, sirohaem synthesis in the plastid to support the function of sulfite reductase is an attractive hypothesis that might explain the retention of some of the tetrapyrrole synthesis enzymes in the *E. longa* plastid. However, analyses of the transcriptome data alone do not provide any clear answer as to whether this hypothesis is valid. Of the various alternative enzymes mediating sirohaem synthesis in various taxa (Tripathy et al. 2010), only two have confidently identified homologs in both *Euglena* spp. (Table S4). One of them is the multifunctional protein CysG, which catalyses all reactions from uroporphyrinogen III to sirohaem, but the respective *Euglena* homolog is devoid of any presequence in either species and is thus most likely cytosolic (Table S4). The other is a stand-alone version of the enzyme (uroporphyrinogen-III C-methyltransferase) catalysing the first step of sirohaem synthesis, called CobA or SirA (Table S4). The *Euglena* homologs exhibit a predicted signal peptide, which is however immediately followed by a region belonging to the mature enzyme, so it is unclear whether this protein is routed to the plastid (indeed it is not among the proteomically confirmed plastid protein in *E. gracilis*). Hence, the role of the enzymes of the tetrapyrrole biosynthesis pathway in the *E. longa* plastid remains unexplained.

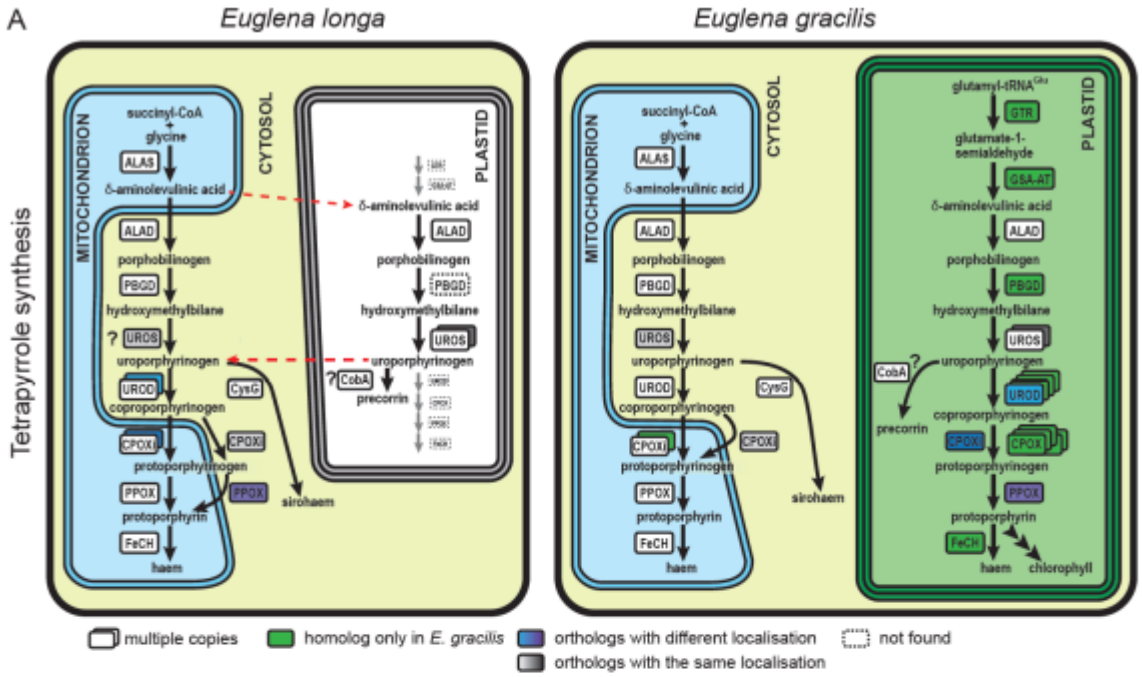

B

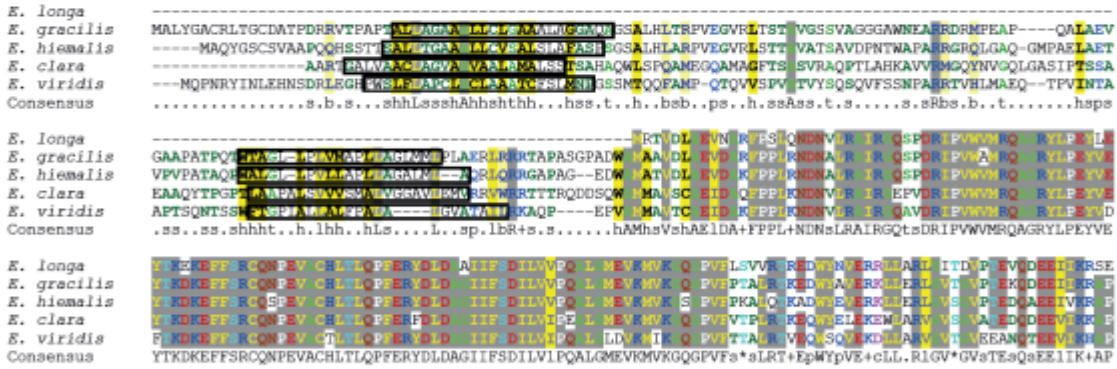

C

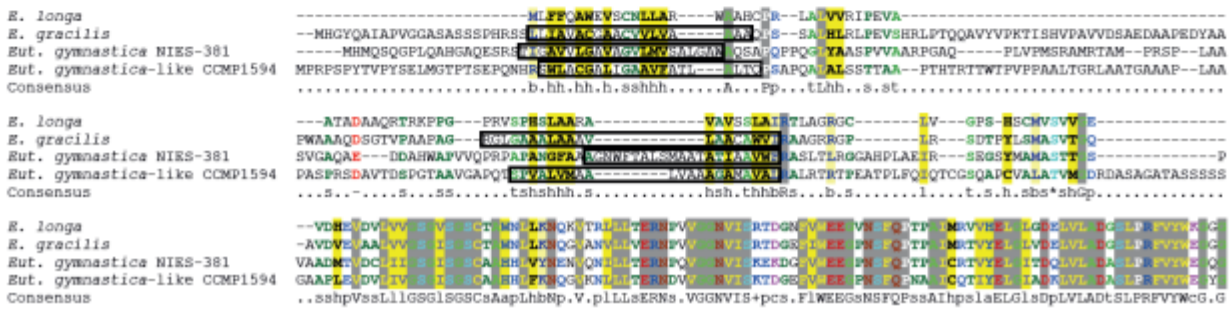

Figure 2: Tetrapyrrole biosynthesis in *E. longa* and *E. gracilis*. A: Schematic comparison of the localization and evolutionary origin of enzymes (see colour-coding graphical legend). Abbreviations: ALAD – delta-aminolevulinate dehydrogenase, ALAS – delta-aminolevulinate synthase, CobA –

uroporphyrinogen-III C-methyltransferase, CPOX – coproporphyrinogen III oxidase, CPOXi – oxygen-independent CPOX, CysG – trifunctional enzyme of sirohaem synthesis (see text), FeCH – ferrochelatase, GSA-AT – glutamate semialdehyde-aminomutase, GTR – glutamyl-tRNA reductase, PBGD – porphobilinogen deaminase, PPOX – protoporphyrinogen oxidase, UROD – uroporphyrinogen decarboxylase, UROS – uroporphyrinogen-III synthase. **B-C:** Sequence alignment of UROD (B) and PPOX (C) presequences, showing the loss of the plastid-targeting motifs in *E. longa*. These targeting motifs represented by transmembrane domains are marked with frames in other euglenophyte sequences.

E. longa plastid does not make fatty acids but maintains phospholipid and glycolipid synthesis

Eukaryotes synthesize even-chain fatty acids by a single large multi-modular fatty acid synthase I (FASI) in the cytosol or by a multi-enzyme type II fatty acid synthesis complex in the plastid. *E. gracilis* possesses both systems (Zimorski et al. 2017). In contrast, *E. longa* encodes only a homolog of the FASI enzyme (Table S5), whereas enzymes of the type II fatty acid synthesis are absent (Fig. 3A) except for the acyl carrier protein (ACP). The loss of plastid-localized fatty acid synthesis in *E. longa* is not without precedent, as it has been also reported for the apicoplast of *Theileria parva* (which is fully dependent on fatty acid supply from host), the plastid of *Perkinsus marinus* (Janouškovec et al. 2015) and the chrysophyte "*Spumella*" sp. NIES-1846 (Dorrell et al. 2019). Nevertheless, the *E. longa* plastid has kept plastid-targeted enzymatic steps downstream of fatty acid synthesis. These include ACP and 4'-phosphopantetheinyl transferases (or holo-ACP synthase) crucial for the synthesis of an active form of ACP, which serves as a carrier of acyl chains in phospholipid and glycolipid biosynthesis (Lambalot and Walsh 1995). Next, *E. longa* possesses predicted plastid-targeted homologs of acyl-ACP synthetases (presumably activating fatty acids imported into the plastid from outside) and all enzymes required for the synthesis of phosphatidic acid (PA) and its subsequent conversion to phosphatidylglycerol (PG) (Fig. 3A; Table S5). It is worth noting that *E. longa* also has a parallel, plastid-independent, route of phosphatidylglycerol synthesis (Table S6).

No other reactions of phospholipid synthesis or decomposition beyond PG synthesis seem to operate in the *E. longa* plastid, but interestingly, we found homologs of the enzymes of the synthesis of galactolipids monogalactosyldiacylglycerol (MGDG) and digalactosyldiacylglycerol (DGDG) in the *E. longa* transcriptome (Fig. 3A, Table S5). All the proteins have a predicted N-terminal plastid-targeting presequence, consistent with the plastidial localization of galactolipid synthesis in all other plastid-bearing eukaryotes studied so far (Yuzawa et al. 2012). In support of the bioinformatic predictions, both MGDG and DGDG could be detected in lipid extracts from *E. longa* and *E. gracilis*, although galactolipid levels were significantly lower in *E. longa* than in the control sample of *E. gracilis* (Fig. 3B). The presence of DGDG was further confirmed by immunofluorescence using an anti-DGDG antibody, which showed DGDG to be present in small foci in the *E. longa* cells (white arrowheads in Fig. 3C), presumably

405 representing individual small plastids. In comparison, most of the volume of the photosynthetic *E. gracilis*
406 cells was stained, whereas the negative control, the primary osmotrophic (i.e. plastid-lacking) euglenoid
407 *Rhabdomonas costata*, did not stain at all.

408 The presence of galactolipids in plastids is generally being explained by their essentiality for the
409 proper functioning of the photosynthetic apparatus, but this view has been challenged by demonstration that
410 cyanobacterial mutants lacking galactolipids can photosynthesize normally (Awai et al. 2001). A
411 photosynthesis-independent role of galactolipids in plastid biology was proposed, too. Transit peptides of
412 plastid-targeted proteins exhibit affinities for MGDG and DGDG in the plastid envelope (Pinnaduwage and
413 Bruce 1996), suggesting a direct role of these lipids in plastid protein import. The photosynthesis-
414 independent role of galactolipids is indicated not only by their presence in the *E. longa* plastid documented
415 here, but also by previous reports from other non-photosynthetic algae, including the diatom *Nitzschia alba*
416 (Anderson et al. 1978) and the chlorophyte *Prototheca wickerhamii* (Borza et al. 2005), and from non-
417 photosynthetic tissues of plants (Awai et al. 2001; Kobayashi 2016). On the other hand, the apicoplast (Botté
418 et al. 2008; Botté et al. 2013) and most likely also the relic plastid of *Helicosporidium* (based on our analysis
419 of the respective genome sequence data generated by Pombert et al. 2014) lack galactolipid synthesis
420 completely. The reason for the differential retention of galactolipids in different colourless plastids remains
421 unclear.

422 In addition to MGDG and DGDG, we identified in samples from both *Euglena* spp. another
423 common glycolipid characteristic for plastids, sulfoquinovosyldiacylglycerol (SQDG) (Fig. 3B) (Hori et al.
424 2016). The presence of SQDG in *E. longa* is also not unprecedented among non-photosynthetic plastid-
425 bearing eukaryotes; see, e.g., its documented occurrence in the diatom *N. alba* or the dinoflagellate *Oxyrrhis*
426 *marina* (Anderson et al. 1978; Goddard-Borger and Williams 2017; Yoon et al. 2017). Of the three enzymes
427 of SQDG biosynthesis normally localized to the plastid, we found in both *Euglena* species only that
428 catalysing the final step (sulfoquinovosyltransferase; Fig. 3A). Interestingly, the standard eukaryotic version
429 of the enzyme, SQD2, is present only in *E. gracilis*, but both species proved to share another isoform
430 phylogenetically affiliated to bacterial SqdX version of the enzyme (Fig. 4). To the best of our knowledge,
431 this is the first encounter of SqdX in any eukaryote. The presence of SQD2 only in *E. gracilis* probably
432 relates to specific needs of its photosynthetic plastid. Indeed, *E. gracilis* contains a much larger amount of
433 SQDG compared to *E. longa* (Fig. 3B) and the profile of esterified fatty acids differs between the two species
434 (*E. longa* lacks SQDG forms with unsaturated longer chains; Table S7).

435 Details of the synthesis of the saccharide moieties of glycolipids in *E. longa* are also worth
436 considering (Fig. 3A). *E. longa* exhibits an ortholog of the *E. gracilis* UDP-glucose epimerase previously
437 identified in the plastid proteome (Table S5), explaining the source of UDP-galactose for galactolipid
438 synthesis. This enzyme seems to have been acquired by euglenophytes from a bacterial source (Fig. S6),

439 but, interestingly, *E. gracilis* encodes another enzyme, which corresponds to the plastidial UDP-glucose
440 epimerase, also called PHD1, known from plants and various algae (Li et al. 2011). The *E. gracilis* PHD1
441 possesses a predicted plastid-targeting presequence (Table S5) and is thus also likely plastidial (although
442 this is not confirmed by proteomic data reported by Novák Vanclová et al. 2019). This putative redundancy
443 in UDP-galactose is apparently not shared by *E. longa*, possibly because of a presumably much lower need
444 for galactolipid synthesis (Fig. 3B). The origin of the SQDG precursor UDP-sulfoquinovose in *E. longa*
445 remains obscure, because as noticed before (Novák Vanclová et al. 2019), euglenophytes in general lack the
446 conventional UDP-sulfoquinovose synthase SQD1/SqdB and probably employ an alternative, unrelated
447 enzyme. UDP-glucose, i.e. the common precursor of both UDP-galactose and UDP-sulfoquinovose, is most
448 likely imported from the cytoplasm, owing to the absence in *E. longa* of a candidate plastid-targeted version
449 of any of the relevant enzymes (UDP-glucose/UDP-sugar pyrophosphorylase).
450

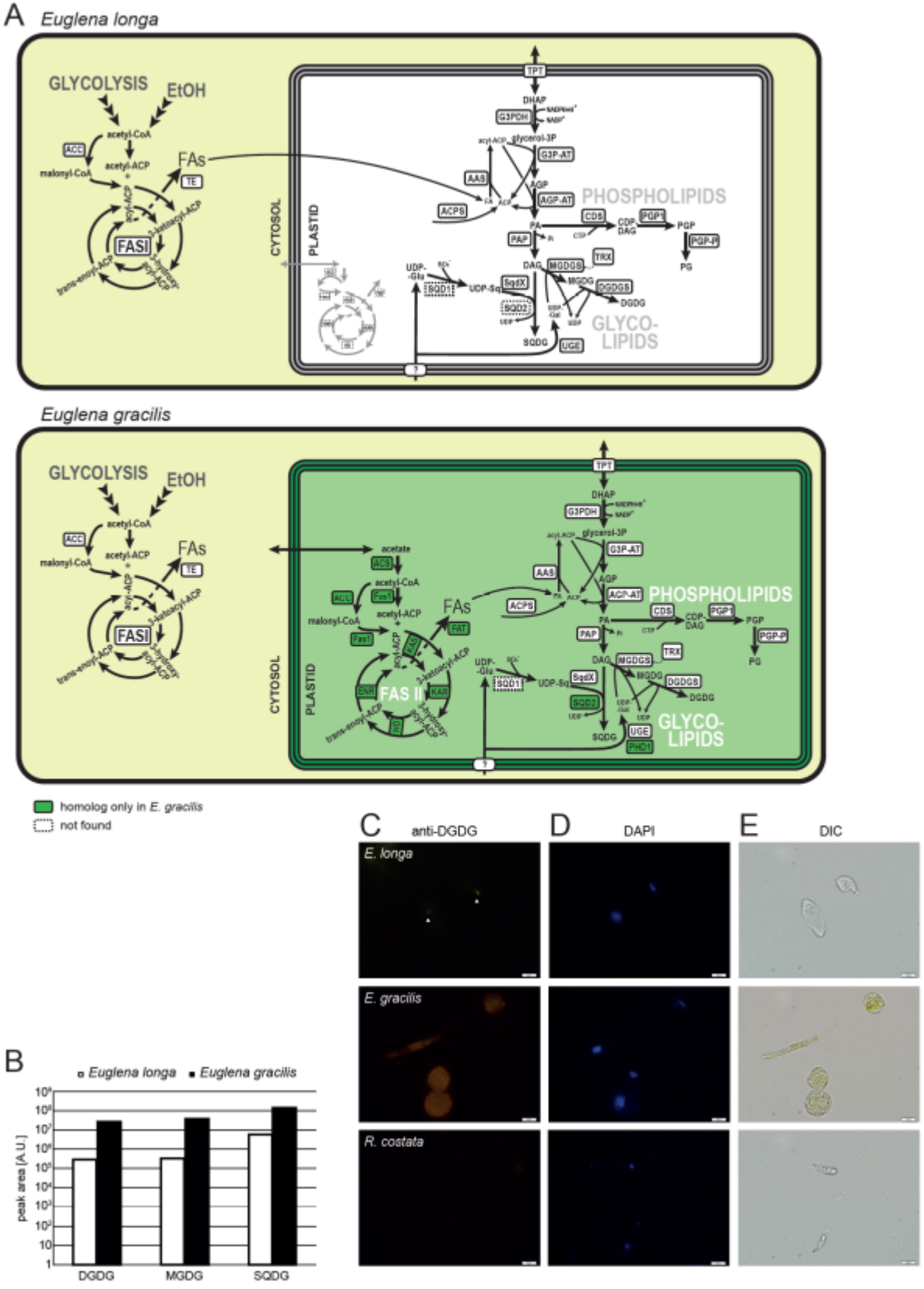

Figure 3: Fatty acid and lipid biosynthesis in *E. longa* and *E. gracilis*. A: Schematic comparison of the

453 localization and evolutionary origin of enzymes. Abbreviations, fatty acid synthesis: ACC – acetyl-CoA
454 carboxylase, ACS – acetyl-CoA synthetase, ENR – enoyl-CoA reductase, Fas1 – malonyl-CoA/acetyl-CoA:
455 ACP transacylase, FASI – type I fatty acid synthase, FAT – fatty acyl-ACP thioesterase, HD – hydroxyacyl-
456 ACP dehydratase, KAR – ketoacyl-ACP reductase, KAS – ketoacyl-ACP synthase, TE – fatty acid
457 thioesterase, TRX – thioredoxin-regulated enzyme; glycolipid synthesis: AAS – acyl-ACP synthase, ACPS
458 – holo-ACP synthase, AGP-AT – acylglycerophosphate acyltransferase, G3P-AT – glycerol-3-phosphate
459 acyltransferase, G3PDH – glycerol-3-phosphate dehydrogenase, MGDG/DGDG – mono-/digalactosyl
460 diacylglycerol, MGDGS/DGDGS – MGDG/DGDG synthase, PAP – phosphatidic acid phosphatase, SQD1
461 – UDP-sulfoquinovose synthase, SQD2/SQDX – sulfoquinovosyl diacylglycerol (SQDG) synthase,
462 UGE/PHD1 – UDP-glucose epimerase, UGP3 – UDP-glucose pyrophosphorylase 3; phospholipid
463 synthesis: CDS – CDP-diacylglycerol synthase, PGP1 – phosphatidylglycerophosphate synthase, PGP-P –
464 phosphateidylglycerophosphate phosphatase. **B:** Semiquantitative comparison of glycolipids present in *E.*
465 *longa* and autotrophic *E. gracilis*. Note the logarithmic scale of the quantification units (peak area). Peak
466 area is an arbitrary unit expressing the intensity of the signal of a particular lipid species, recalculated
467 according to their respective ionization promptitude. As each lipid species have different ionization
468 promptitude, note that direct comparison can be done only within lipid class (for details, see Tomčala et al.
469 2017). **C-E:** Immunofluorescence micrographs using anti-DGDG antibody (C), DAPI (D) and differential
470 interference contrast (E). Autotrophic *E. gracilis* represents a positive control, while the aplastidic
471 euglenozoan *R. costata* was used as negative control.
472

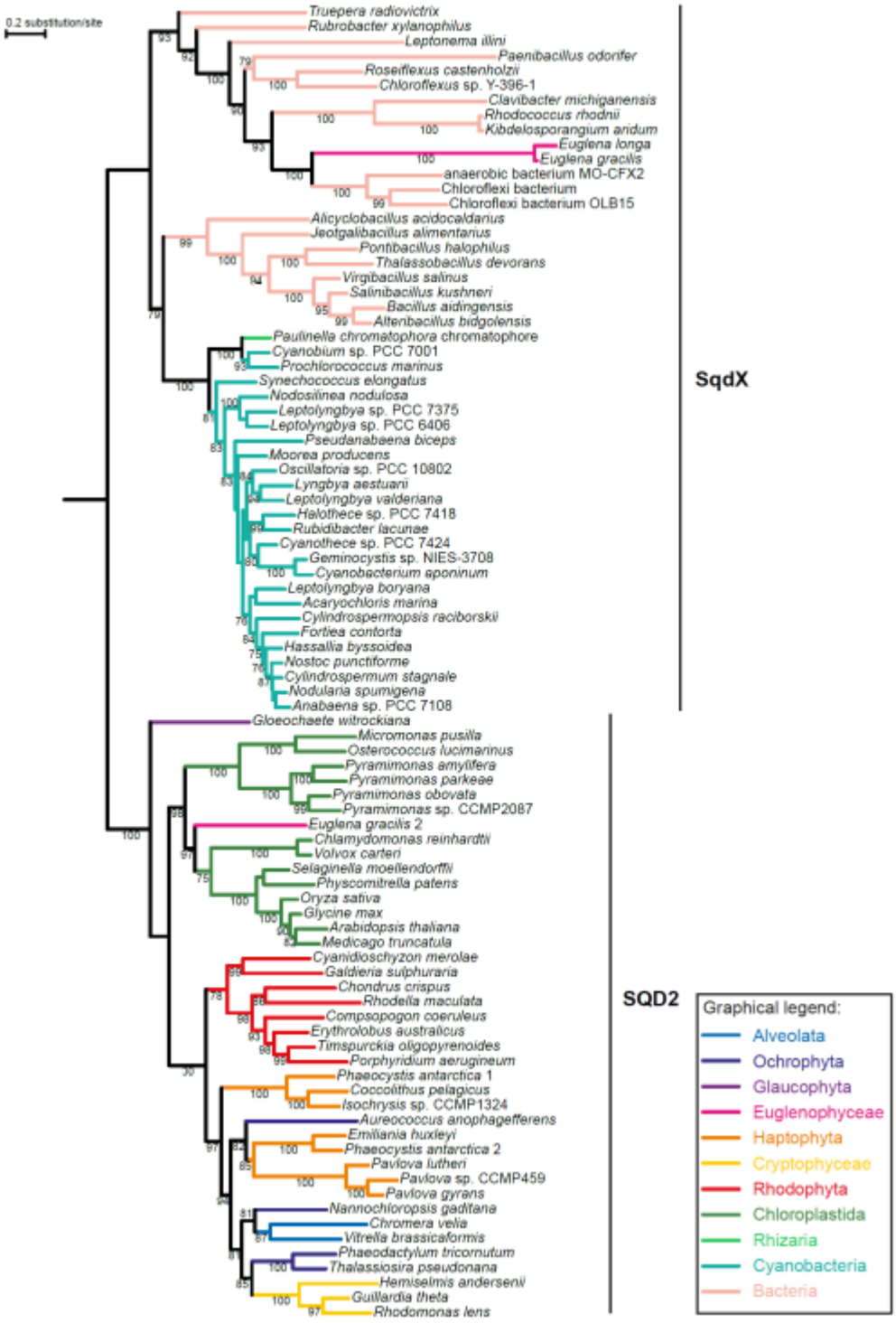

Figure 4: Euglenophytes have replaced the eukaryotic form of sulfoquinovosyltransferase (SQD2) with a bacterial version (SqdX). The maximum-likelihood tree was inferred with IQ-TREE using the LG+F+G4 substitution model and ultra-fast bootstrapping. The UFboot support values are indicated at branches when higher than 75%.

A linearized Calvin-Benson pathway in the *E. longa* plastid

The presence of genes encoding both subunits of the enzyme RuBisCO in *E. longa* (Záhonová et al. 2016) raises the question whether the Calvin-Benson cycle (CBC) as a whole has been preserved in this organism to provide ribulose-1,5-bisphosphate, the RuBisCO substrate. A putative *E. longa* plastid triose-phosphate isomerase was described previously (Sun et al. 2008). We confirmed not only this candidate, but additionally identified homologs with putative plastid-targeting presequences for almost all remaining CBC enzymes (Table S8). Our identification was confirmed by phylogenetic analyses (supplementary Dataset S1), which showed specific relationships of the *E. longa* proteins to the previously characterized CBC enzymes from other euglenophytes (Markunas and Triemer 2016). However, two key CBC enzymes are apparently missing from the *E. longa* transcriptome: phosphoglycerate kinase (ptPGK) and glyceraldehyde-phosphate dehydrogenase (ptGAPDH). The homologs of these enzymes present in *E. longa* are not orthologous to the plastid-targeted isoenzymes from other euglenophytes and all clearly lack a plastid-targeting presequence (Table S8). Hence, these are presumably cytosolic enzymes involved in glycolysis/gluconeogenesis. The lack of ptPGK and ptGAPDH in *E. longa* means that the product of the RuBisCO carboxylase activity, 3-phosphoglycerate (3PG), cannot be converted (via 2,3-bisphosphoglycerate; 2,3-BPG) to glyceraldehyde-3-phosphate (GA3P) in the plastid and the cycle becomes a linear pathway (Fig. 5).

Assuming that the reactions catalyzed by fructose bisphosphatase, phosphoribulokinase, and RuBisCO are not reversible (Raines and Lloyd 2001), the flux through this linearized CB pathway most likely goes from GA3P to 3PG, with a net production of six molecules of 3PG from five molecules of GA3P due to fixation of three CO_2 molecules catalysed by RuBisCO. We thus need to define the origin of GA3P entering the pathway. Euglenophytes do not store starch in the plastid (instead they have cytosolic paramylon as a storage polysaccharide; Kiss et al. 1987), and indeed we did not find any glucose metabolism-related enzymes in the predicted *E. longa* plastid proteome. Hence, GA3P cannot be produced by a glycolytic route in the *E. longa* plastid. The presence of the plastid-targeted glycerophosphate dehydrogenase (Table S5) in principle allows for generation of GA3P from glycerol-3-phosphate (via dihydroxyacetone phosphate; DHAP; Fig. 3), which could possibly come from the degradation of glycerolipids in the plastid. However, no phospholipid-degradation enzymes (phospholipases) appear to localize to the plastid in *E. longa*. Hence, the primary function of glycerophosphate dehydrogenase is perhaps to operate in the reverse direction, i.e. to provide glycerol-3-phosphate for the plastid phospholipid and glycolipid synthesis (see above). The *E. longa* plastid thus most likely imports GA3P or DHAP from the cytosol (Fig. 5). This assumption is supported by the presence of several members of the plastid phosphate translocator (pPT) family (Fig. S7; Facchinelli and Weber 2011), including one phylogenetically closest to a previously characterized cryptophyte transporter with a preference for DHAP (Haferkamp et al. 2006). Concerning the opposite end of the hypothesized linear CB pathway, we did not identify any

candidate *E. longa* plastid-targeted enzyme that would metabolize 3PG further (see the absence of 3PG dehydrogenase discussed above), so this intermediate is most likely exported from the plastid into the cytosol, probably also by one of the members of the pPT family of transporters (Fig. 5).

The operation of CBC is inherently linked with the oxygenase side-activity of RuBisCO, which converts ribulose-1,5-bisphosphate into 3PG and phosphoglycolate instead of two molecules of 3PG that are produced by the regular carboxylase activity (Tabita et al. 2007). Phosphoglycolate is metabolized in the photorespiration pathway, initiated by phosphoglycolate phosphatase yielding glycolate. We did find a candidate plastid-targeted phosphoglycolate phosphatase in *E. longa* (Table S8), orthologous to a protein detected in *E. gracilis* plastid proteome, suggesting that the *E. longa* RuBisCO has the oxygenase activity and phosphoglycolate is metabolized in this species. However, we did not find in our *E. longa* transcriptome assembly any discernible homolog of the recently characterized transporter PLGG1 mediating glycolate export from the plastid in the canonical photorespiratory pathway (Pick et al. 2013), although *E. gracilis* does have it (Table S8). Since there is no obvious candidate for a plastid-targeted glycolate-metabolizing enzyme (glycolate oxidase, glyoxylate reductase, glycolaldehyde dehydrogenase) in *E. longa*, it is unclear how glycolate is removed from the plastid of this species. It is possible that the amount of glycolate produced in the *E. longa* plastid is low and that it can be exported by an alternative (PLGG1-independent) route, whose existence has been proposed also for plant plastids (Walker et al. 2016) and which might be sufficient for glycolate recycling in the semi-parasitic plant *Cuscuta campestris* capable of low-efficiency photosynthesis (Vogel et al. 2018).

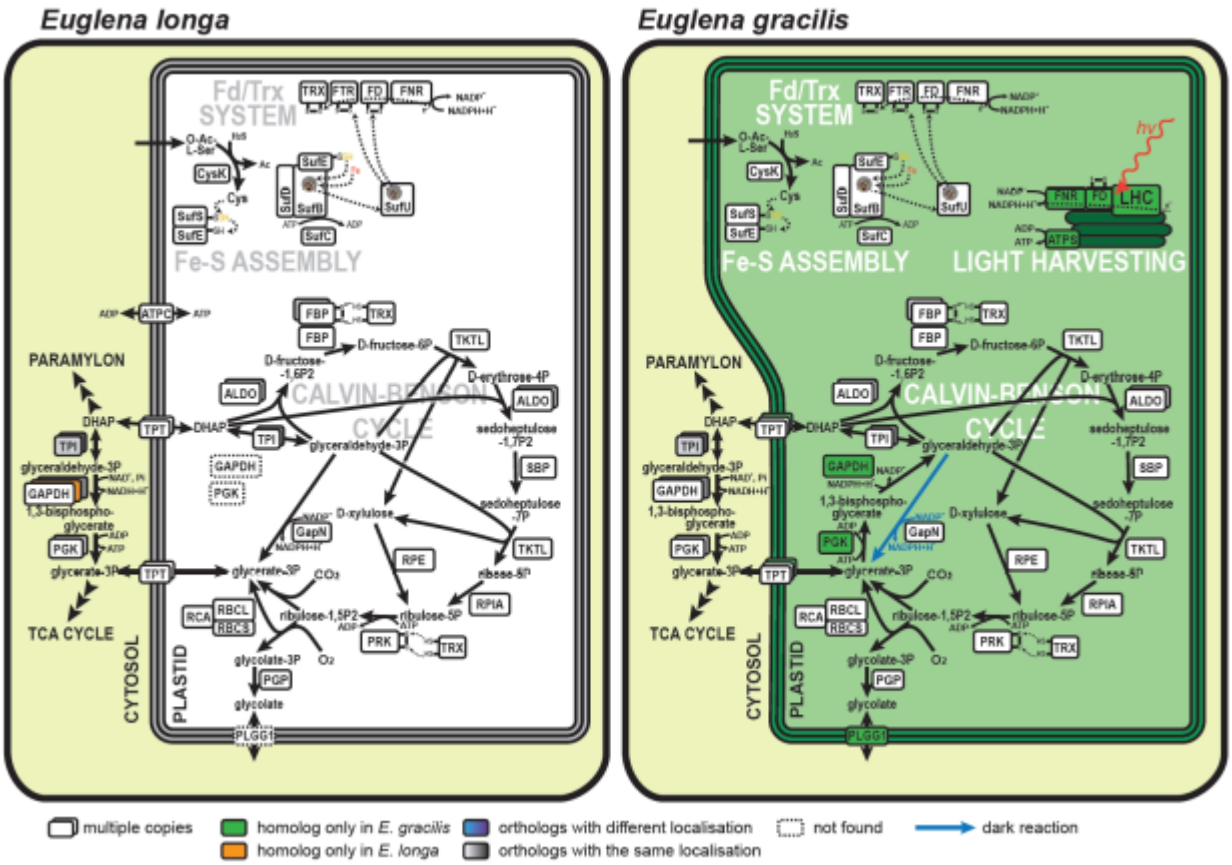

Figure 5: Carbon metabolism in the plastids of *E. longa* and *E. gracilis*. The Calvin-Benson cycle (CBC) resident to this organelle is central to the plastid carbon metabolism, regulated by the ferredoxin/thioredoxin (Fd/Trx) system. Reduction of disulfide bonds by the Fd/Trx system activates FBP and PRK. FTR and FD of the Fd/Trx system require for their function a post-translationally added Fe-S prosthetic group provided by the Fe-S assembly system. GapN apparently mediates shuttling of reducing equivalent (NADPH) through the exchange of DHAP/GA3P and 3PG, reflecting the cytosolic NADPH/$NADP^+$ ratio and thus an overall metabolic state of the cell. In contrast, *E. gracilis* plastid is an energy-converting organelle, harvesting light into chemical energy bound as NADPH and ATP and subsequently using this bound energy to fix CO_2 into organic carbohydrates via the CBC. Enzyme abbreviations are colour-coded according to their inferred evolutionary origin, see the graphical legend. Abbreviations, CBC: ALDO – aldolase, DHAP – dihydroxyacetone-phosphate, FBP – fructose-1,6-bisphosphatase, GAPDH – glyceraldehyde-3-phosphate dehydrogenase, PGK – 3-phosphoglygerate kinase, PGP – phosphoglycolate phosphatase, PLGG1 – plastid glycolate/glycerate transporter, PRK – phosphoribulokinase, RBCL/RBCS – RuBisCO large/small subunit, RCA – RuBisCO activase, RPE – ribulose-5-phosphate epimerase; RPIA – ribulose-phosphate isomerase A, SBP – sedoheptulose-1,7-bisphosphatase, TKTL – transketolase, TPI – triose-phosphate isomerase, TPT – triose-phosphate translocator; Fd/Trx system: FD – ferredoxin; FNR – FD/NADP+ oxidoreductase, FTR

– FD/TRX oxidoreductase, TRX – thioredoxin, ATPS – ATP synthase, ATPC – ADP/ATP translocase, LHC – light-harvesting complex.

The system of redox regulation of the Calvin-Benson pathway is conserved in *E. longa*

Although the photosynthetic machinery, including all photosystem I subunits, is missing from *E. longa* (Záhonová et al. 2018), we found homologs (with clear plastidial localization) of the typical "photosynthetic" (PetF-related) ferredoxin (Fd) and ferredoxin-$NADP^+$ reductase (FNR) (Table S9). These two proteins are primarily involved in passing electrons from an activated photosystem I to $NADP^+$, which is thus reduced to NADPH, the main donor of reducing equivalents for anabolic reactions in the plastid (above all, CO_2 fixation). Phylogenetic analysis of FNR homologs from euglenophytes revealed the existence of two different, yet related, clades affiliated to FNR from green algae (Fig. 6). One clade comprises the *E. longa* FNR plus its orthologs from photosynthetic euglenophytes (*E. gracilis* and two *Eutreptiella* strains), whereas the second clade is restricted to the photosynthetic species. Two different FNR forms also exist in plants, one functioning in photosynthesis (production of NADPH dependent on the function of the photosystem I; marked with "P" in Fig. 6) and the other being a "non-photosynthetic" homolog ("NP" in Fig. 6) that allows the electron flow in the reverse direction, from NADPH to Fd (Vollmer et al. 2001). In analogy with plants, we suggest that the two euglenophyte FNR clades functionally differ, with one (that lacking a representative in *E. longa*) serving in photosynthesis and the other (present in *E. longa*) mediating light-independent production of reduced Fd.

Multiple plastid enzymes depend on reduced Fd as an electron donor, namely glutamate synthase, lipid desaturases, nitrite reductase, and sulfite reductase (Neuhaus and Emes 2000). As discussed in previous sections, glutamate synthase and nitrite reductase are missing from *E. longa*, whereas all identified lipid desaturases are predicted as targeted to the mitochondrion or the ER (Table S5). A two-subunit sulfite reductase seems to be present in the plastid of *E. gracilis* (Novák Vanclová et al. 2019) and both subunits have highly similar homologs in *E. longa* (Table S4), but this form of the enzyme utilizes NADPH rather than ferredoxin as electron donor (Patron et al. 2008).

Another crucial role of Fd in plastids is to provide electrons to ferredoxin:thioredoxin reductase (FTR) mediating reduction of the protein thioredoxin (Trx). The Fd/Trx system regulates several plastid CBC enzymes in response to the redox status in the stroma and, in extension, to the photosynthetic activity of the plastid (Fig. 5). An excess of NADPH leads to electrons being relayed from reduced ferredoxin to the Fd/Trx system, which eventually reduces certain disulfide bonds in the target enzymes, thus changing their activity (Schürmann and Buchanan 2008). This ensures activation of the CBC only when the photosynthetic machinery works properly. Notably, FTR and Trx homologs with evident plastid-targeting presequences are both present in *E. longa* (Table S9). Specific motifs necessary for the function of the Fd/Trx system

584 (Schürmann and Buchanan 2008) are conserved in the respective *E. longa* proteins (Fig. S8), consistent with
585 the Fd/Trx system being functional in this species. In addition, two *E. longa* CB pathway enzymes, fructose
586 bisphosphatase (two of the three isoforms present) and phosphoribulokinase, exhibit the conserved Trx
587 regulatory cysteine motifs similar to their orthologs in *E. gracilis* (Fig. S8, Table S10). Thus, we suggest
588 that the CB pathway in *E. longa* is sensitive to the redox status in the plastid, specifically to the concentration
589 of NADPH (Fig. 5).
590

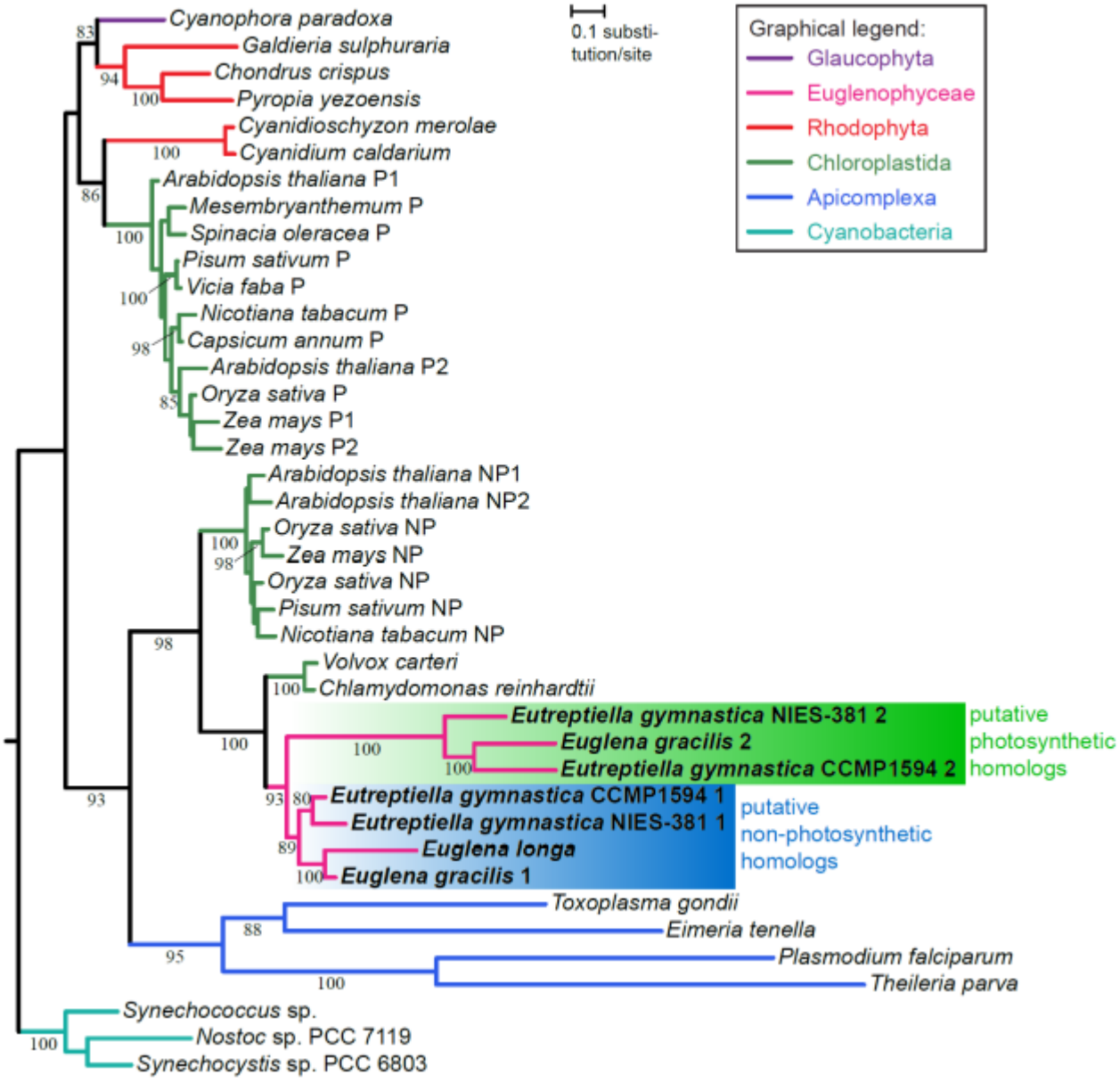

591
592 **Figure 6: The inferred phylogeny of FNR.** The maximum-likelihood tree was inferred with IQ-TREE
593 using the LG+F+G4 substitution model and ultra-fast bootstrapping. The UFboot support values are

indicated at branches when higher than 75%. Euglenophyte species are in bold, and their putative photosynthetic and non-photosynthetic homologs are depicted. P, photosynthetic; NP, non-photosynthetic.

May the *E. longa* plastid be involved in keeping the redox balance of the cell?

How to interpret in functional terms the retention of the linearized CB pathway and its putative redox regulation in the non-photosynthetic plastid of *E. longa*? The key role of the pathway is supported by the fact that production of the large RuBisCO subunit seems to be the *raison d'être* for the preservation of the plastid genome in *E. longa* (Záhonová et al. 2016). The presence of CB enzymes in a non-photosynthetic plastid is not without precedent, as it has been reported from a set of unrelated colourless algae and plants. Some of them, e.g. the dinoflagellate *Crypthecodinium cohnii*, the dictyochophytes *Pteridomonas danica* and *Ciliophrys infusionum*, the cryptophyte *Cryptomonas paramecium*, and some parasitic or mycoheterotrophic land plants, are known to encode RuBisCO (Sekiguchi et al. 2002; Sanchez-Puerta et al. 2007; Donaher et al. 2009; Wicke et al. 2013; Hadariová et al. 2018), but how complete is the complement of other CBC enzymes in these species is unknown. In contrast, transcriptomic or genomic analyses of other colourless plastid-bearing taxa, such as the dinoflagellate *Pfiesteria piscicida*, the green alga *Helicosporidium* sp. ATCC50920, the diatom *Nitzschia* sp. NIES-3581, and the non-photosynthetic chrysophytes, revealed the presence of a subset of CB enzymes, including ptPGK and ptGAPDH, but not of RuBisCO (Kim et al. 2013; Pombert et al. 2014; Kamikawa et al. 2017; Graupner et al. 2018). Hence, the constellation of the CB enzymes retained in the *E. longa* plastid seems to be unique.

The CBC enzymes retained in various non-photosynthetic eukaryotes obviously do not serve to sustain autotrophic growth, as ATP and the reducing power generated by photosynthesis are unavailable. The CB pathway in *Nitzschia* sp. NIES-3581 was proposed to serve as a source of erythrose-4-P for the synthesis of aromatic amino acid via the shikimate pathway in the plastid (Kamikawa et al. 2017). Although not discussed in the respective report (Pombert et al. 2014), the CB pathway in the *Helicosporidium* plastid may likewise serve to feed the co-localized shikimate pathway with erythrose-4-P. However, such a rationalization of the CB pathway in the *E. longa* plastid would not work, since enzymes for aromatic amino acid biosynthesis in this species are apparently localized to the cytosol (Table S2) and thus have access to erythrose-4-P produced by the pentose phosphate pathway. In addition, the need to produce erythrose-4-P in the *E. longa* plastid would not explain the retention of RuBisCO (absent in both *Nitzschia* and *Helicosporidium*). A photosynthesis- and CBC-independent role of RuBisCO was described in oil formation in developing seeds of *Brassica napus*, where refixation of CO_2 released during carbohydrate-to-fatty acid conversion increases carbon use efficiency (Schwender et al. 2004). A similar explanation is unlikely to hold for RuBisCO retention in *E. longa*, given the lack of fatty acid synthesis in its plastid and the apparently much smaller significance of oil as a reserve substance in *E. longa* compared to *B. napus*.

We believe that the identification of the putatively functional Fd/Trx system, despite the absence of the photosynthetic electron transport chain in this species, provides one of the key hints to understanding the physiological role of the linear CB pathway in the *E. longa* plastid. The second potentially important piece of the puzzle is provided by the proteomic data from *E. gracilis* (Novák Vanclová et al. 2019), which indicated the presence of a unique form of GAPDH, the so-called non-phosphorylating GAPDH also referred to as GapN, in the plastid (Table S8). This enzyme uses $NADP^+$ to directly oxidize GA3P to 3PG, skipping the intermediate 2,3-BPG (and hence not leading to ATP generation) and producing NADPH rather than NADH (Iddar et al. 2003). In plants, this enzyme is localized to the cytosol and is involved in shuttling of reducing equivalents from the plastid by the exchange of GA3P and 3PG between the two compartments (Rius et al. 2006). *E. longa* possesses a GapN homolog highly similar to the *E. gracilis* protein, including an N-terminal presequence (Table S8), consistent with its presumed plastidial localization. It thus appears that in *Euglena* spp. GapN mediates shuttling of reducing equivalents in the opposite direction than in plants, i.e. from the cytosol to the plastid (Fig. 5). In case of *E. longa* this may be the main (if not the only) mechanism of providing NADPH for the use in the plastid, whereas *E. gracilis* would utilize it when photosynthetic production of NADPH is shut down. At the same time, the shuttle provides a mechanism of linking the level of NADPH in the plastid with the cytosolic concentration of GA3P.

Taken together, we propose that in *E. longa* (at specific circumstances possibly also in *E. gracilis*) the plastidial NADPH/$NADP^+$ ratio is directly influenced by the redox status of the cell, i.e. that it rises in an excess of reducing power that slows down the glycolytic oxidation of GA3P in the cytosol. This stimulates the linear CB pathway via the Fd/Trx system, effectively decreasing the level of GA3 by converting it to 3PG without further increasing the reducing power in the cell. This conclusion is apparent from considering the overall stoichiometries of the two alternative pathways from GA3 to 3PG:

glycolysis: $5\ GA3P + 5\ NAD^+ + 5\ ADP + 5\ PO_3^{2-} \rightarrow 5\ 3PG + 5\ NADH + 5\ H^+ + 5\ ATP$

CB pathway: $5\ GA3P + 3\ CO_2 + 3\ H_2O + 3\ ATP \rightarrow 6\ 3PG + 3\ ADP + 2\ PO_3^{2-}$

The key difference is that the CB pathway does not produce NADH that needs to be reoxidized to keep the glycolytic pathway running, since the fixed CO_2 effectively serves as an electron acceptor. Hence, turning the CB bypass on may help the cell keep the redox balance when reoxidation of NADH is not efficient, e.g. at hypoxic (or anoxic) conditions (although this happens at the expense of ATP). Indeed, euglenophytes in their natural settings are probably often exposed to the shortage of oxygen, and anaerobiosis in *E. gracilis* has been studied to some extent (Tucci et al. 2010; Zimorski et al. 2017). The anaerobic heterotrophic metabolism of *E. gracilis* relies on fermentative degradation of the reserve polysaccharide paramylon leading to production of wax esters (Yoshida et al. 2016). It is likely that *E. longa* exhibits a similar metabolic adaptation to low levels of ambient oxygen as *E. gracilis*. However, details of the euglenophyte anaerobic metabolism need to be worked out yet, and we propose that the plastid may be involved in it as a

kind of a redox valve. Work is ongoing to test this hypothesis and to illuminate further details of physiological role of the linear CB pathway in the *E. longa* plastid.

Conclusions

Endosymbiotic organelles have proven to be extremely evolutionarily versatile. One of the manifestations is the recurrent loss of key metabolic functions of the canonical forms of both mitochondria and plastids, resulting in anaerobic mitochondria-related organelles (such as hydrogenosomes and mitosomes) and non-photosynthetic plastids distributed across diverse eukaryotic branches. A lot of attention has been paid to various mitochondrial derivatives and it is now well documented that they vary substantially in the complement of functional pathways they have retained (Roger et al. 2017). The variation in functional profiles of non-photosynthetic plastids is less well known, as the only example studied in detail is the apicoplast of apicomplexan parasites. Nevertheless, a picture is emerging that independently evolved colourless plastids may also exhibit a surprising degree of diversity in terms of their metabolic capacity.

Our analyses of the *E. longa* plastid stretch the breadth of variation among non-photosynthetic plastids even further. The combination of pathways present (tocopherol and phylloquinone synthesis, glycolipid synthesis and a linearized CB pathway including RuBisCO), absent (fatty acid, amino acid, and isoprenoid precursor synthesis), and potentially residual (tetrapyrrole synthesis) makes the *E. longa* plastid unlike any of the previously investigated non-photosynthetic plastids, including the apicoplast. However, further work, combining additional *in silico* analyses (aimed, e.g., at potential plastid membrane transporters mediating metabolite exchange with the cytosol) with biochemical and cytological investigations is needed to achieve a more precise idea about the protein composition of the *E. longa* plastid and a better understanding of its physiological roles.

Materials and Methods

Identification and annotation of plastid-targeted proteins

The analyses reported in this study were done using the *E. longa* transcriptome assembly reported previously (Záhonová et al. 2018). Protein models for annotation were generated by a custom Geneious 8.1.6 (Kearse et al. 2012) script that extracted all open reading frames longer than 297 bp, translated the sequences and then filtered the protein models by a local BLAST+ ver.2.2.30 (Altschul et al. 1997) search against the Swiss-Prot database (version 10/5/15, max E-value=10). Transcript models containing at least a partial spliced leader sequence (TTTTTCG) at their 5'-end or 3'-end (within the first or last 35 nt) were translated in the forward or reverse direction only, respectively.

Candidates for plastid-targeted proteins were identified using criteria for prediction of plastid-targeting presequences described in detail by Záhonová et al. (2018). In the first step protein sequences were gathered that fulfilled at least one of the following requirements: (i) the signal peptide was predicted by the PrediSi v.2004 (Hiller et al. 2004) or PredSL v.2005 (Petsalaki et al. 2006) standalone programs; (ii) one or two transmembrane domains at the N-terminus of the protein were predicted by standalone TMHMM 2.0c (online version where graphical output was considered) (Krogh et al. 2001). The resulting set was then filtered by checking for the presence of a plastid transit peptide, which was predicted by standalone MultiLoc2.5 (Blum et al. 2009) after an *in silico* removal of the signal peptide or the first transmembrane domain. Finally, protein models with a putative plastid-targeting presequence were automatically annotated using InterProScan 5.21 (Jones et al. 2014) and the annotations were manually scrutinized to identify proteins with an assignable specific metabolism-related function (enzymes of the metabolism of nucleic acids and proteins were ignored in this study).

In parallel we searched with BLAST v.2.2.30 (including tBLASTn against the transcriptome assembly and, in special cases, even against the whole set of raw RNAseq reads) for putative plastid proteins by direct identification and evaluation of homologs of enzymes of specific biochemical pathways potentially localized to the plastid; as queries we used respective protein sequences from *E. gracilis* (as identified by Novák Vanclová et al. 2019), reference sequences from the KEGG PATHWAY Database (https://www.genome.jp/kegg/pathway.html), or sequences identified by literature searches. In some cases, a more sensitive homology detection algorithm HMMER 3.0 (Mistry et al. 2013) to identify homologs of poorly conserved enzymes (e.g., UROS). For comparative purposes we used the same approach to identify plastid-targeted proteins encoded by the transcriptome assemblies from *E. gracilis* reported by (Yoshida et al. 2016) (accession GDJR00000000.1) and (Ebenezer et al. 2017) (accession GEFR00000000.1). Where accessions are given for *E. gracilis* sequences, those starting with GDJR and GEFR belong to the former and latter dataset, respectively.

For MenA cDNA resequencing, RNA was isolated using TRI Reagent (Thermo Fisher Scientific, San Jose, USA) and mRNA was then extracted using the Dynabeads mRNA Purification kit (Thermo Fisher Scientific). Reverse-transcription was performed with random hexamers and StrataScript III Reverse Transcriptase (Thermo Fisher Scientific). For cDNA amplification, forward 5'-GGTGCTGTTCTGCTCTCACT-3' and reverse 5'-CAGTGGGGATCAGAGATGCG-3' primers, and the Q5 High-Fidelity DNA polymerase in a standard buffer (New England Biolabs) were used. Amplicons were purified on MinElute PCR Purification columns (Qiagen, Hilden, Germany) and sequenced at the GATC sequencing facility (Konstanz, Germany). The MenA cDNA sequence is deposited in GenBank with the accession number MK484704.

730 **Phylogenetic analyses**

731 Phylogenetic analyses were employed to establish orthologous relationships among *E. longa* and *E. gracilis*
732 genes or to illuminate the origin of the euglenophyte proteins of special interest. Homologs of target proteins
733 were identified by BLAST v.2.2.30 searches in the non-redundant protein sequence database at NCBI
734 (www.ncbi.nlm.nih.gov) and among protein models of selected organisms from JGI (Joint Genome
735 Institute, jgi.doe.gov) and MMETSP (Marine Microbial Eukaryote Transcriptome Sequencing Project,
736 marinemicroeukaryotes.org; Keeling et al. 2014). Sequences were aligned using the MAFFT v7.407
737 (Multiple Alignment using Fast Fourier Transform) tool with L-INS-I setting (Katoh and Standley 2013)
738 and poorly aligned positions were eliminated by the trimAL v1.4.rev22 tool with "-automated1" trimming
739 (Capella-Gutierrez et al. 2009). For presentation purposes, alignments were processed using the CHROMA
740 software (Goodstadt and Ponting 2001). Maximum likelihood (ML) trees were inferred from the alignments
741 using the LG+F+G4 model of IQ-TREE v1.6.9 (Nguyen et al. 2015), and employing the strategy of rapid
742 bootstrapping followed by a "thorough" ML search with 1,000 bootstrap replicates (-m TEST -bb 1000).
743 The list of species, and the number of sequences and amino acid positions are present in Tables S11-S22 for
744 each phylogenetic tree.
745
746 **Culture conditions**
747 *Euglena gracilis* strain *Z* ("autotrophic" conditions) were cultivated statically under constant illumination
748 at 26 °C in Cramer-Myers medium supplemented with ethanol (0.8% v/v) as a carbon source (Cramer and
749 Myers 1952). *E. longa* strain CCAP 1204-17a (a gift from W. Hachtel, Bonn, Germany) and heterotrophic
750 *E. gracilis* strain *Z* were cultivated in identical medium without illumination. The cultures of *E. longa* were
751 not completely axenic, but the contaminating bacteria were kept at as low level as possible. *Rhabdomonas*
752 *costata* strain PANT2 was provided by Vladimír Hampl (Department of Parasitology, Faculty of Science,
753 Charles University in Prague, Czech Republic). It was isolated from a freshwater body in Pantanal (Brasil)
754 and grown with an uncharacterised mixture of bacteria in Sonneborn's *Paramecium* medium (pH 7.4;
755 Sonneborn 1950) at room temperature (inoculated every three to four weeks).
756
757 **Mass spectrometry of structural lipids and terpenoids**
758 For analysis of structural lipids, extracts from *E. longa* and autotrophic *E. gracilis* cellular pellets (four
759 biological samples of different culture age) were obtained with chloroform and methanol solution (ratio –
760 2:1) following the method of (Folch et al. 1957) as modified by (Košťál and Šimek 1998). Samples were
761 homogenized in extraction solution with glass beads using TissueLyser LT mill (Qiagen). Homogenates
762 were dried, weighted, and resolved in 500 µl of chloroform and methanol (1:2) with internal standard PC
763 17:0/17:0 (Sigma Aldrich). Aliquots from each sample extract were used for lipid determination by HPLC

using a liquid chromatograph and autosampler Accela (Thermo Fisher Scientific). The samples (5 µL) were injected and separated on the Gemini column 250 × 2 mm; i.d. 3 µm (Phenomenex, Torrance, USA). A linear ion trap LTQ-XL mass spectrometer (Thermo Fisher Scientific) was used in both positive and negative ion ESI mode. The settings of the system followed the methodology published earlier (Tomčala et al. 2017). Data were acquired and processed using Xcalibur software version 2.1 (Thermo Fisher Scientific). Particular compounds were determined based on m/z value, retention time, behaviour in positive and negative ionization mode, and characteristic fragmentation pattern of target molecules (for details see Tomčala et al. 2017).

Terpenoids were extracted from an autotrophic culture of *E. gracilis*, a heterotrophic culture of *E. gracilis*, and a culture of *E. longa* of the same age in three repetitions. The same extraction procedure as for lipid analysis was used. Sample aliquots were injected into the high-resolution mass spectrometry system powered by Orbitrap Q-Exactive Plus with Dionex Ultimate 3000 XRS pump and Dionex Ultimate 3000 XRS Open autosampler (all by Thermo Fisher Scientific) and followed the settings described in (Tomčala et al. 2017). Data were acquired and processed using Xcalibur software version 2.1. Identification of OH-PhQ was achieved by considering the m/z value, fragmentation pattern, and high-resolution data. Tocopherols (α, β/γ, and δ) were determined by the same characteristic as OH-PhQ and results were then compared with commercially purchased standards (α-tocopherol from Sigma Aldrich, the other three variants from SUPELCO).

Immunofluorescence assay

Immunofluorescence was performed as described previously (Botté et al. 2011). Briefly, cells were fixed in 4% paraformaldehyde for 30 minutes, cellular membranes were permeabilized for 10 minutes on ice with 0.1% non-ionic detergent Igepal CA-630 (Sigma-Aldrich) in PHEM buffer pH 6.9 (60 mM PIPES, 25 mM HEPES, 10 mM EGTA, 2 mM $MgCl_2$), and background was masked with 3% BSA in PHEM buffer. DGDG was detected using a polyclonal rabbit anti-DGDG antibody (1:25) that was a kind gift from Cyrille Y. Botté (ApicoLipid Team, Laboratoire Adaptation et Pathogenie des Microorganismes, University of Grenoble I, France), followed by incubation with a secondary Cy3-labeled polyclonal goat anti-rabbit antibody (AP132C, 1:800, Merck Millipore, Billerica, USA). To improve the fluorescence lifetime, Fluoroshield™ with DAPI mounting medium (Sigma-Aldrich) was used. Cells were mounted on slides and observed with a fluorescent microscope Olympus BX53 (Olympus, Tokyo, Japan). Photosynthetic *E. gracilis* served as a positive control, and the primary osmotroph (i.e. aplastidic) *R. costata* as a negative control.

Acknowledgements

We thank Vladimír Hampl (Charles University) for providing the culture of *Rhabdomonas costata* and Cyrille Y. Botté (University of Grenoble I) for providing the anti-DGDG antibody. We acknowledge computation resources provided by CERIT-SC and MetaCentrum, Brno, Czech Republic, and the infrastructure grant "Přístroje IET" (CZ.1.05/2.1.00/19.0388). We thank Laboratory of Analytical Biochemistry and Metabolomics (Biology Centre, Czech Academy of Sciences) for free access to LC–MS instruments. This study was supported by the Czech Science Foundation grants 17-21409S (to ME) and 16-24027S (to MO), the Czech Academy of Sciences fellowship (to ZF), and the Scientific Grant Agency of the Slovak Ministry of Education (grant VEGA 1/0535/17 to JK). This work was also part of the project "Centre for research of pathogenicity and virulence of parasites", supported by the European Regional Development Fund, within the Operational programme for Research, Development and Education (CZ.02.1.01/0.0/0.0/16_019/0000759).

Competing interests

The authors declare that they have no financial or non-financial competing interests.

References

Altschul, SF, Madden, TL, Schaffer, AA, Zhang, J, Zhang, Z, Miller, W, Lipman, DJ. 1997. Gapped BLAST and PSI-BLAST: a new generation of protein database search programs. Nucleic Acids Res 25:3389-3402.

Anderson, R, Livermore, BP, Kates, M, Volcani, BE. 1978. The lipid composition of the non-photosynthetic diatom *Nitzschia alba*. Biochim Biophys Acta 528:77-88.

Awai, K, Maréchal, E, Block, MA, Brun, D, Masuda, T, Shimada, H, Takamiya, K, Ohta, H, Joyard, J. 2001. Two types of MGDG synthase genes, found widely in both 16:3 and 18:3 plants, differentially mediate galactolipid syntheses in photosynthetic and nonphotosynthetic tissues in *Arabidopsis thaliana*. Proc Natl Acad Sci U S A 98:10960-10965.

Blum, T, Briesemeister, S, Kohlbacher, O. 2009. MultiLoc2: integrating phylogeny and Gene Ontology terms improves subcellular protein localization prediction. BMC Bioinformatics 10:274.

Borza, T, Popescu, CE, Lee, RW. 2005. Multiple metabolic roles for the nonphotosynthetic plastid of the green alga *Prototheca wickerhamii*. Eukaryot Cell 4:253-261.

Botté, C, Saidani, N, Mondragon, R, Mondragon, M, Isaac, G, Mui, E, McLeod, R, Dubremetz, JF, Vial, H, Welti, R, et al. 2008. Subcellular localization and dynamics of a digalactolipid-like epitope in *Toxoplasma gondii*. J Lipid Res 49:746-762.

831 Botté, CY, Yamaryo-Botté, Y, Janouškovec, J, Rupasinghe, T, Keeling, PJ, Crellin, P, Coppel, RL,
832 Maréchal, E, McConville, MJ, McFadden, GI. 2011. Identification of plant-like galactolipids in
833 *Chromera velia*, a photosynthetic relative of malaria parasites. J Biol Chem 286:29893-29903.
834 Botté, CY, Yamaryo-Botté, Y, Rupasinghe, TW, Mullin, KA, MacRae, JI, Spurck, TP, Kalanon, M, Shears,
835 MJ, Coppel, RL, Crellin, PK, et al. 2013. Atypical lipid composition in the purified relict plastid
836 (apicoplast) of malaria parasites. Proc Natl Acad Sci U S A 110:7506-7511.
837 Brettel, K. 1997. Electron transfer and arrangement of the redox cofactors in photosystem I. Biochimica et
838 Biophysica Acta (BBA) - Bioenergetics 1318:322-373.
839 Capella-Gutierrez, S, Silla-Martinez, JM, Gabaldon, T. 2009. trimAl: a tool for automated alignment
840 trimming in large-scale phylogenetic analyses. Bioinformatics 25:1972-1973.
841 Cenci, U, Qiu, H, Pillonel, T, Cardol, P, Remacle, C, Colleoni, C, Kadouche, D, Chabi, M, Greub, G,
842 Bhattacharya, D, et al. 2018. Host-pathogen biotic interactions shaped vitamin K metabolism in
843 Archaeplastida. Sci Rep 8:15243.
844 Cihlář, J, Füssy, Z, Horák, A, Oborník, M. 2016. Evolution of the tetrapyrrole biosynthetic pathway in
845 secondary algae: conservation, redundancy and replacement. PLOS ONE 11:e0166338.
846 Cramer, M, Myers, J. 1952. Growth and photosynthetic characteristics of *Euglena gracilis*. Archiv
847 Mikrobiol 17:384-402.
848 Dagenais-Bellefeuille, S, Morse, D. 2013. Putting the N in dinoflagellates. Front Microbiol 4:369.
849 Dailey, HA, Dailey, TA, Gerdes, S, Jahn, D, Jahn, M, O'Brian, MR, Warren, MJ. 2017. Prokaryotic heme
850 biosynthesis: Multiple pathways to a common essential product. Microbiol Mol Biol Rev 81.
851 Disch, A, Schwender, J, Muller, C, Lichtenthaler, HK, Rohmer, M. 1998. Distribution of the mevalonate
852 and glyceraldehyde phosphate/pyruvate pathways for isoprenoid biosynthesis in unicellular algae
853 and the cyanobacterium *Synechocystis* PCC 6714. Biochem J 333 (Pt 2):381-388.
854 Donaher, N, Tanifuji, G, Onodera, NT, Malfatti, SA, Chain, PS, Hara, Y, Archibald, JM. 2009. The
855 complete plastid genome sequence of the secondarily nonphotosynthetic alga *Cryptomonas*
856 *paramecium*: reduction, compaction, and accelerated evolutionary rate. Genome Biol Evol 1:439-
857 448.
858 Dorrell, RG, Azuma, T, Nomura, M, Audren de Kerdrel, G, Paoli, L, Yang, S, Bowler, C, Ishii, KI,
859 Miyashita, H, Gile, GH, et al. 2019. Principles of plastid reductive evolution illuminated by
860 nonphotosynthetic chrysophytes. Proc Natl Acad Sci U S A 116:6914-6923.
861 Ebenezer, TE, Carrington, M, Lebert, M, Kelly, S, Field, MC. 2017. *Euglena gracilis* genome and
862 transcriptome: Organelles, nuclear genome assembly strategies and initial features. Adv Exp Med
863 Biol 979:125-140.
864 Fatihi, A, Latimer, S, Schmollinger, S, Block, A, Dussault, PH, Vermaas, WF, Merchant, SS, Basset, GJ.

2015. A dedicated type II NADPH dehydrogenase performs the penultimate step in the biosynthesis of vitamin K_1 in *Synechocystis* and *Arabidopsis*. Plant Cell 27:1730-1741.

Fernandez, E, Galvan, A. 2008. Nitrate assimilation in *Chlamydomonas*. Eukaryot Cell 7:555-559.

Fernández Robledo, JA, Caler, E, Matsuzaki, M, Keeling, PJ, Shanmugam, D, Roos, DS, Vasta, GR. 2011. The search for the missing link: a relic plastid in *Perkinsus*? Int J Parasitol 41:1217-1229.

Figueroa-Martinez, F, Nedelcu, AM, Smith, DR, Reyes-Prieto, A. 2015. When the lights go out: the evolutionary fate of free-living colorless green algae. New Phytologist 206:972-982.

Folch, J, Lees, M, Sloane Stanley, GH. 1957. A simple method for the isolation and purification of total lipides from animal tissues. J Biol Chem 226:497-509.

Furt, F, Oostende, Cv, Widhalm, JR, Dale, MA, Wertz, J, Basset, GJC. 2010. A bimodular oxidoreductase mediates the specific reduction of phylloquinone (vitamin K1) in chloroplasts. Plant J 64:38-46.

Füssy, Z, Oborník, M. 2017. Chapter Six - Chromerids and Their Plastids. In: Y Hirakawa, editor. Advances in Botanical Research: Academic Press. p. 187-218.

Füssy Z, Faitová T, Oborník M. 2019. Subcellular compartments interplay for carbon and nitrogen allocation in *Chromera velia* and *Vitrella brassicaformis*. Genom Biol Evol, in press. doi:10.1093/gbe/evz123.

Gerdes, S, Lerma-Ortiz, C, Frelin, O, Seaver, SM, Henry, CS, de Crecy-Lagard, V, Hanson, AD. 2012. Plant B vitamin pathways and their compartmentation: a guide for the perplexed. J Exp Bot 63:5379-5395.

Giordano, M, Raven, JA. 2014. Nitrogen and sulfur assimilation in plants and algae. Aquatic Botany 118:45-61.

Gockel, G, Hachtel, W. 2000. Complete gene map of the plastid genome of the nonphotosynthetic euglenoid flagellate *Astasia longa*. Protist 151:347-351.

Gockel, G, Hachtel, W, Baier, S, Fliss, C, Henke, M. 1994. Genes for components of the chloroplast translational apparatus are conserved in the reduced 73-kb plastid DNA of the nonphotosynthetic euglenoid flagellate *Astasia longa*. Curr Genet 26:256-262.

Goddard-Borger, ED, Williams, SJ. 2017. Sulfoquinovose in the biosphere: occurrence, metabolism and functions. Biochem J 474:827-849.

Gomez-Silva, B, Timko, MP, Schiff, JA. 1985. Chlorophyll biosynthesis from glutamate or 5-aminolevulinate in intact *Euglena* chloroplasts. Planta 165:12-22.

Goodstadt, L, Ponting, CP. 2001. CHROMA: consensus-based colouring of multiple alignments for publication. Bioinformatics 17:845-846.

Graupner, N, Jensen, M, Bock, C, Marks, S, Rahmann, S, Beisser, D, Boenigk, J. 2018. Evolution of heterotrophy in chrysophytes as reflected by comparative transcriptomics. FEMS Microbiol Ecol

94.

Gu, X, Harding, S, Nyamdari, B, Aulakh, K, Clermont, K, Westwood, J, Tsai, C-J. 2018. A role for phylloquinone biosynthesis in the plasma membrane as revealed in a non-photosynthetic parasitic plant. bioRxiv:257519.

Gutbrod, K, Romer, J, Dormann, P. 2019. Phytol metabolism in plants. Prog Lipid Res 74:1-17.

Hadariová, L, Vesteg, M, Birčák, E, Schwartzbach, SD, Krajčovič, J. 2017. An intact plastid genome is essential for the survival of colorless *Euglena longa* but not *Euglena gracilis*. Curr Genet 63:331-341.

Hadariová, L, Vesteg, M, Hampl, V, Krajčovič, J. 2018. Reductive evolution of chloroplasts in non-photosynthetic plants, algae and protists. Curr Genet 64:365-387.

Haferkamp, I, Deschamps, P, Ast, M, Jeblick, W, Maier, U, Ball, S, Neuhaus, HE. 2006. Molecular and biochemical analysis of periplastidial starch metabolism in the cryptophyte *Guillardia theta*. Eukaryot Cell 5:964-971.

Hachtel, W. 1996. DNA and gene expression in nonphotosynthetic plastids. In: M Pessarakli, editor. Handbook of Photosynthesis. New York: Marcel Dekker. p. 349-355.

Hiller, K, Grote, A, Scheer, M, Munch, R, Jahn, D. 2004. PrediSi: prediction of signal peptides and their cleavage positions. Nucleic Acids Res 32:W375-379.

Hori, K, Nobusawa, T, Watanabe, T, Madoka, Y, Suzuki, H, Shibata, D, Shimojima, M, Ohta, H. 2016. Tangled evolutionary processes with commonality and diversity in plastidial glycolipid synthesis in photosynthetic organisms. Biochim Biophys Acta 1861:1294-1308.

Iddar, A, Valverde, F, Serrano, A, Soukri, A. 2003. Purification of recombinant non-phosphorylating NADP-dependent glyceraldehyde-3-phosphate dehydrogenase from *Streptococcus pyogenes* expressed in *E. coli*. Mol Cell Biochem 247:195-203.

Jackson, C, Knoll, AH, Chan, CX, Verbruggen, H. 2018. Plastid phylogenomics with broad taxon sampling further elucidates the distinct evolutionary origins and timing of secondary green plastids. Sci Rep 8:1523.

Janouškovec, J, Horák, A, Oborník, M, Lukeš, J, Keeling, PJ. 2010. A common red algal origin of the apicomplexan, dinoflagellate, and heterokont plastids. Proc Natl Acad Sci U S A 107:10949-10954.

Janouškovec, J, Tikhonenkov, DV, Burki, F, Howe, AT, Kolísko, M, Mylnikov, AP, Keeling, PJ. 2015. Factors mediating plastid dependency and the origins of parasitism in apicomplexans and their close relatives. Proc Natl Acad Sci U S A 112:10200-10207.

Jones, P, Binns, D, Chang, HY, Fraser, M, Li, W, McAnulla, C, McWilliam, H, Maslen, J, Mitchell, A, Nuka, G, et al. 2014. InterProScan 5: genome-scale protein function classification. Bioinformatics 30:1236-1240.

933 Kamikawa, R, Moog, D, Zauner, S, Tanifuji, G, Ishida, KI, Miyashita, H, Mayama, S, Hashimoto, T, Maier,
934 UG, Archibald, JM, et al. 2017. A non-photosynthetic diatom reveals early steps of reductive
935 evolution in plastids. Mol Biol Evol 34:2355-2366.
936 Karamoko, M, Cline, S, Redding, K, Ruiz, N, Hamel, PP. 2011. Lumen thiol oxidoreductase1, a disulfide
937 bond-forming catalyst, is required for the assembly of photosystem II in *Arabidopsis*. The Plant
938 Cell 23:4462.
939 Katoh, K, Standley, DM. 2013. MAFFT multiple sequence alignment software version 7: improvements in
940 performance and usability. Mol Biol Evol 30:772-780.
941 Ke, H, Sigala, PA, Miura, K, Morrisey, JM, Mather, MW, Crowley, JR, Henderson, JP, Goldberg, DE,
942 Long, CA, Vaidya, AB. 2014. The heme biosynthesis pathway is essential for *Plasmodium*
943 *falciparum* development in mosquito stage but not in blood stages. J Biol Chem 289:34827-34837.
944 Kearse, M, Moir, R, Wilson, A, Stones-Havas, S, Cheung, M, Sturrock, S, Buxton, S, Cooper, A,
945 Markowitz, S, Duran, C, et al. 2012. Geneious Basic: an integrated and extendable desktop software
946 platform for the organization and analysis of sequence data. Bioinformatics 28:1647-1649.
947 Keeling, PJ. 2013. The number, speed, and impact of plastid endosymbioses in eukaryotic evolution. Annu
948 Rev Plant Biol 64:583-607.
949 Keeling, PJ, Burki, F, Wilcox, HM, Allam, B, Allen, EE, Amaral-Zettler, LA, Armbrust, EV, Archibald,
950 JM, Bharti, AK, Bell, CJ, et al. 2014. The Marine Microbial Eukaryote Transcriptome Sequencing
951 Project (MMETSP): illuminating the functional diversity of eukaryotic life in the oceans through
952 transcriptome sequencing. PLOS Biol 12:e1001889.
953 Kim, D, Filtz, MR, Proteau, PJ. 2004. The methylerythritol phosphate pathway contributes to carotenoid
954 but not phytol biosynthesis in *Euglena gracilis*. J Nat Prod 67:1067-1069.
955 Kim, GH, Jeong, HJ, Yoo, YD, Kim, S, Han, JH, Han, JW, Zuccarello, GC. 2013. Still acting green:
956 continued expression of photosynthetic genes in the heterotrophic Dinoflagellate *Pfiesteria*
957 *piscicida* (Peridiniales, Alveolata). PLOS ONE 8:e68232.
958 Kiss, JZ, Vasconcelos, AC, Triemer, RE. 1987. Structure of the euglenoid storage carbohydrate, paramylon.
959 Am J Bot 74:877-882.
960 Kitaoka, S, Nakano, Y, Miyatake, K, Yokota, A. 1989. Enzymes and their functional location. In: DE
961 Buetow, editor. Subcellular Biochemistry and Molecular Biology: Academic Press. p. 1-135.
962 Kivic, PA, Vesk, M. 1974. An electron microscope search for plastids in bleached *Euglena gracilis* and in
963 *Astasia longa*. Can J Bot 52:695-699.
964 Kobayashi, K. 2016. Role of membrane glycerolipids in photosynthesis, thylakoid biogenesis and
965 chloroplast development. J Plant Res 129:565-580.
966 Kořený, L, Oborník, M. 2011. Sequence evidence for the presence of two tetrapyrrole pathways in *Euglena*

gracilis. Genome Biol Evol 3:359-364.

Košťál, V, Šimek, P. 1998. Changes in fatty acid composition of phospholipids and triacylglycerols after cold-acclimation of an aestivating insect prepupa. Journal of Comparative Physiology B 168:453-460.

Krajčovič, J, Ebringer, L, Schwartzbach, SD. 2002. Reversion of endosymbiosis? In: J Seckbach, editor. Symbiosis: Mechanisms and model systems. Dordrecht: Springer Netherlands. p. 185-206.

Krogh, A, Larsson, B, von Heijne, G, Sonnhammer, EL. 2001. Predicting transmembrane protein topology with a hidden Markov model: application to complete genomes. J Mol Biol 305:567-580.

Kwong, WK, Del Campo, J, Mathur, V, Vermeij, MJA, Keeling, PJ. 2019. A widespread coral-infecting apicomplexan with chlorophyll biosynthesis genes. Nature 568:103-107.

Lakey, B, Triemer, R. 2016. The tetrapyrrole synthesis pathway as a model of horizontal gene transfer in euglenoids. J Phycol 53:198-217.

Lambalot, RH, Walsh, CT. 1995. Cloning, overproduction, and characterization of the *Escherichia coli* holo-acyl carrier protein synthase. J Biol Chem 270:24658-24661.

Leander, BS, Lax, G, Karnkowska, A, Simpson, AGB. 2017. Euglenida. In: JM Archibald, AGB Simpson, CH Slamovits, L Margulis, M Melkonian, DJ Chapman, JO Corliss, editors. Handbook of the Protists. Cham: Springer International Publishing. p. 1-42.

Li, C, Wang, Y, Liu, L, Hu, Y, Zhang, F, Mergen, S, Wang, G, Schlappi, MR, Chu, C. 2011. A rice plastidial nucleotide sugar epimerase is involved in galactolipid biosynthesis and improves photosynthetic efficiency. PLoS Genet 7:e1002196.

Lim, L, McFadden, GI. 2010. The evolution, metabolism and functions of the apicoplast. Philos Trans R Soc Lond B Biol Sci 365:749-763.

Lohr, M, Schwender, J, Polle, JE. 2012. Isoprenoid biosynthesis in eukaryotic phototrophs: a spotlight on algae. Plant Sci 185-186:9-22.

Lochner, K, Doring, O, Bottger, M. 2003. Phylloquinone, what can we learn from plants? Biofactors 18:73-78.

Maeda, H, DellaPenna, D. 2007. Tocopherol functions in photosynthetic organisms. Curr Opin Plant Biol 10:260-265.

Marin, B, Palm, A, Klingberg, M, Melkonian, M. 2003. Phylogeny and taxonomic revision of plastid-containing euglenophytes based on SSU rDNA sequence comparisons and synapomorphic signatures in the SSU rRNA secondary structure. Protist 154:99-145.

Markunas, CM, Triemer, RE. 2016. Evolutionary history of the enzymes involved in the Calvin-Benson cycle in euglenids. J Eukaryot Microbiol 63:326-339.

Martins-Duarte, ES, Carias, M, Vommaro, R, Surolia, N, de Souza, W. 2016. Apicoplast fatty acid synthesis

1001 is essential for pellicle formation at the end of cytokinesis in *Toxoplasma gondii*. J Cell Sci
1002 129:3320-3331.
1003 Matsuzaki, M, Kuroiwa, H, Kuroiwa, T, Kita, K, Nozaki, H. 2008. A cryptic algal group unveiled: a plastid
1004 biosynthesis pathway in the oyster parasite *Perkinsus marinus*. Mol Biol Evol 25:1167-1179.
1005 McFadden, GI. 2014. Origin and evolution of plastids and photosynthesis in eukaryotes. Cold Spring Harb
1006 Perspect Biol 6:a016105.
1007 McFadden, GI, Yeh, E. 2017. The apicoplast: now you see it, now you don't. Int J Parasitol 47:137-144.
1008 Miller, LH, Ackerman, HC, Su, XZ, Wellems, TE. 2013. Malaria biology and disease pathogenesis: insights
1009 for new treatments. Nat Med 19:156-167.
1010 Mistry, J, Finn, RD, Eddy, SR, Bateman, A, Punta, M. 2013. Challenges in homology search: HMMER3
1011 and convergent evolution of coiled-coil regions. Nucleic Acids Res 41:e121.
1012 Moffatt, BA, Ashihara, H. 2002. Purine and pyrimidine nucleotide synthesis and metabolism. Arabidopsis
1013 Book 1:e0018.
1014 Moore, RB, Oborník, M, Janouškovec, J, Chrudimský, T, Vancová, M, Green, DH, Wright, SW, Davies,
1015 NW, Bolch, CJ, Heimann, K, et al. 2008. A photosynthetic alveolate closely related to apicomplexan
1016 parasites. Nature 451:959-963.
1017 Nagaraj, VA, Sundaram, B, Varadarajan, NM, Subramani, PA, Kalappa, DM, Ghosh, SK, Padmanaban, G.
1018 2013. Malaria parasite-synthesized heme is essential in the mosquito and liver stages and
1019 complements host heme in the blood stages of infection. PLOS Pathog 9:e1003522.
1020 Neuhaus, HE, Emes, MJ. 2000. Nonphotosynthetic metabolism in plastids. Annu Rev Plant Physiol Plant
1021 Mol Biol 51:111-140.
1022 Nguyen, LT, Schmidt, HA, von Haeseler, A, Minh, BQ. 2015. IQ-TREE: a fast and effective stochastic
1023 algorithm for estimating maximum-likelihood phylogenies. Mol Biol Evol 32:268-274.
1024 Novák Vanclová, AMG, Zoltner, M, Kelly, S, Soukal, P, Záhonová, K, Füssy, Z, Ebenezer, TE, Lacová
1025 Dobáková, E, Eliáš, M, Lukeš, J, et al. 2019. Proteome of the secondary plastid of *Euglena gracilis*
1026 reveals several metabolic quirks and traces of a colourful history. bioRxiv:573709.
1027 Nudelman, MA, Rossi, MS, Conforti, V, Triemer, RE. 2003. Phylogeny of Euglenophyceae based on small
1028 subunit rDNA sequences: Taxonomic implications. J Phycol 39:226-235.
1029 Oborník, M, Green, BR. 2005. Mosaic origin of the heme biosynthesis pathway in photosynthetic
1030 eukaryotes. Mol Biol Evol 22:2343-2353.
1031 Oborník, M, Janouškovec, J, Chrudimský, T, Lukeš, J. 2009. Evolution of the apicoplast and its hosts: from
1032 heterotrophy to autotrophy and back again. Int J Parasitol 39:1-12.
1033 Oda, Y, Miyatake, K, Kitaoka, S. 1979. Inability of *Euglena gracilis* Z to utilize nitrate, nitrite and urea as
1034 the nitrogen sources. Bulletin of the University of Osaka Prefecture. Series B. Agriculture and

1035 Biology 31:43-48.
1036 Patron, NJ, Durnford, DG, Kopriva, S. 2008. Sulfate assimilation in eukaryotes: fusions, relocations and
1037 lateral transfers. BMC Evol Biol 8:39.
1038 Petsalaki, EI, Bagos, PG, Litou, ZI, Hamodrakas, SJ. 2006. PredSL: a tool for the N-terminal sequence-
1039 based prediction of protein subcellular localization. Genomics Proteomics Bioinformatics 4:48-55.
1040 Pick, TR, Brautigam, A, Schulz, MA, Obata, T, Fernie, AR, Weber, AP. 2013. PLGG1, a plastidic glycolate
1041 glycerate transporter, is required for photorespiration and defines a unique class of metabolite
1042 transporters. Proc Natl Acad Sci U S A 110:3185-3190.
1043 Pinnaduwage, P, Bruce, BD. 1996. In vitro interaction between a chloroplast transit peptide and chloroplast
1044 outer envelope lipids is sequence-specific and lipid class-dependent. J Biol Chem 271:32907-
1045 32915.
1046 Pombert, JF, Blouin, NA, Lane, C, Boucias, D, Keeling, PJ. 2014. A lack of parasitic reduction in the
1047 obligate parasitic green alga *Helicosporidium*. PLoS Genet 10:e1004355.
1048 Ponce-Toledo, RI, Deschamps, P, Lopez-Garcia, P, Zivanovic, Y, Benzerara, K, Moreira, D. 2017. An
1049 Early-Branching Freshwater Cyanobacterium at the Origin of Plastids. Curr Biol 27:386-391.
1050 Raines, CA, Lloyd, JC. 2001. C3 carbon reduction cycle. eLS: John Wiley & Sons, Ltd.
1051 Rius, SP, Casati, P, Iglesias, AA, Gomez-Casati, DF. 2006. Characterization of an *Arabidopsis thaliana*
1052 mutant lacking a cytosolic non-phosphorylating glyceraldehyde-3-phosphate dehydrogenase. Plant
1053 Mol Biol 61:945-957.
1054 Roger, AJ, Muñoz-Gómez, SA, Kamikawa, R. 2017. The origin and diversification of mitochondria. Curr
1055 Biol 27:R1177-R1192.
1056 Sanchez-Puerta, MV, Lippmeier, JC, Apt, KE, Delwiche, CF. 2007. Plastid genes in a non-photosynthetic
1057 dinoflagellate. Protist 158:105-117.
1058 Sanz-Luque, E, Chamizo-Ampudia, A, Llamas, A, Galvan, A, Fernandez, E. 2015. Understanding nitrate
1059 assimilation and its regulation in microalgae. Front Plant Sci 6:899.
1060 Seeger, JW, Bentley, R. 1991. Phylloquinone (vitamin K_1) biosynthesis in *Euglena gracilis* strain *Z*.
1061 Phytochemistry 30:3585-3589.
1062 Sekiguchi, H, Moriya, M, Nakayama, T, Inouye, I. 2002. Vestigial chloroplasts in heterotrophic
1063 stramenopiles *Pteridomonas danica* and *Ciliophrys infusionum* (Dictyochophyceae). Protist
1064 153:157-167.
1065 Shashidhara, LS, Smith, AG. 1991. Expression and subcellular location of the tetrapyrrole synthesis enzyme
1066 porphobilinogen deaminase in light-grown *Euglena gracilis* and three nonchlorophyllous cell lines.
1067 Proc Natl Acad Sci U S A 88:63-67.
1068 Schopfer, P, Heyno, E, Drepper, F, Krieger-Liszkay, A. 2008. Naphthoquinone-dependent generation of

superoxide radicals by quinone reductase isolated from the plasma membrane of soybean. Plant Physiol 147:864.

Schürmann, P, Buchanan, BB. 2008. The ferredoxin/thioredoxin system of oxygenic photosynthesis. Antioxid Redox Signal 10:1235-1274.

Schwender, J, Goffman, F, Ohlrogge, JB, Shachar-Hill, Y. 2004. Rubisco without the Calvin cycle improves the carbon efficiency of developing green seeds. Nature 432:779-782.

Siemeister, G, Buchholz, C, Hachtel, W. 1990a. Genes for ribosomal proteins are retained on the 73 kb DNA from *Astasia longa* that resembles *Euglena* chloroplast DNA. Curr Genet 18:457-464.

Siemeister, G, Buchholz, C, Hachtel, W. 1990b. Genes for the plastid elongation factor Tu and ribosomal protein S7 and six tRNA genes on the 73 kb DNA from *Astasia longa* that resembles the chloroplast DNA of *Euglena*. Mol Gen Genet 220:425-432.

Slamovits, CH, Keeling, PJ. 2008. Plastid-derived genes in the nonphotosynthetic alveolate *Oxyrrhis marina*. Mol Biol Evol 25:1297-1306.

Smith, DR, Lee, RW. 2014. A plastid without a genome: evidence from the nonphotosynthetic green algal genus *Polytomella*. Plant Physiol 164:1812-1819.

Sonneborn, TM. 1950. Methods in the general biology and genetics of *Paramecium aurelia*. Journal of Experimental Zoology 113:87-147.

Sun, GL, Shen, W, Wen, JF. 2008. Triosephosphate isomerase genes in two trophic modes of euglenoids (euglenophyceae) and their phylogenetic analysis. J Eukaryot Microbiol 55:170-177.

Ševčíková, T, Horák, A, Klimeš, V, Zbránková, V, Demir-Hilton, E, Sudek, S, Jenkins, J, Schmutz, J, Přibyl, P, Fousek, J, et al. 2015. Updating algal evolutionary relationships through plastid genome sequencing: did alveolate plastids emerge through endosymbiosis of an ochrophyte? Sci Rep 5:10134.

Tabita, FR, Hanson, TE, Li, H, Satagopan, S, Singh, J, Chan, S. 2007. Function, structure, and evolution of the RubisCO-like proteins and their RubisCO homologs. Microbiol Mol Biol Rev 71:576-599.

Tomčala, A, Kyselová, V, Schneedorferová, I, Opekarová, I, Moos, M, Urajová, P, Kručinská, J, Oborník, M. 2017. Separation and identification of lipids in the photosynthetic cousins of Apicomplexa *Chromera velia* and *Vitrella brassicaformis*. J Sep Sci 40:3402-3413.

Tripathy, BC, Sherameti, I, Oelmuller, R. 2010. Siroheme: an essential component for life on earth. Plant Signal Behav 5:14-20.

Tucci, S, Vacula, R, Krajčovič, J, Proksch, P, Martin, W. 2010. Variability of wax ester fermentation in natural and bleached *Euglena gracilis* strains in response to oxygen and the elongase inhibitor flufenacet. J Eukaryot Microbiol 57:63-69.

Turmel, M, Gagnon, MC, O'Kelly, CJ, Otis, C, Lemieux, C. 2009. The chloroplast genomes of the green

algae *Pyramimonas*, *Monomastix*, and *Pycnococcus* shed new light on the evolutionary history of prasinophytes and the origin of the secondary chloroplasts of euglenids. Mol Biol Evol 26:631-648.

Van Dingenen, J, Blomme, J, Gonzalez, N, Inzé, D. 2016. Plants grow with a little help from their organelle friends. J Exp Bot 67:6267-6281.

Vogel, A, Schwacke, R, Denton, AK, Usadel, B, Hollmann, J, Fischer, K, Bolger, A, Schmidt, MH, Bolger, ME, Gundlach, H, et al. 2018. Footprints of parasitism in the genome of the parasitic flowering plant *Cuscuta campestris*. Nat Commun 9:2515.

Vollmer, M, Thomsen, N, Wiek, S, Seeber, F. 2001. Apicomplexan parasites possess distinct nuclear-encoded, but apicoplast-localized, plant-type ferredoxin-NADP+ reductase and ferredoxin. J Biol Chem 276:5483-5490.

Walker, BJ, South, PF, Ort, DR. 2016. Physiological evidence for plasticity in glycolate/glycerate transport during photorespiration. Photosynth Res 129:93-103.

Waller, RF, Gornik, SG, Kořený, L, Pain, A. 2016. Metabolic pathway redundancy within the apicomplexan-dinoflagellate radiation argues against an ancient chromalveolate plastid. Commun Integr Biol 9:e1116653.

Watanabe, F, Yoshimura, K, Shigeoka, S. 2017. Biochemistry and physiology of vitamins in *Euglena*. In: SD Schwartzbach, S Shigeoka, editors. *Euglena*: Biochemistry, Cell and Molecular Biology. Cham: Springer International Publishing. p. 65-90.

Webster, DA, Hackett, DP, Park, RB. 1967. The respiratory chain of colorless algae: III. Electron microscopy. J Ultrastruct Res 21:514-523.

Wedel, N, Soll, J, Paap, BK. 1997. CP12 provides a new mode of light regulation of Calvin cycle activity in higher plants. Proc Natl Acad Sci U S A 94:10479-10484.

Weinstein, JD, Beale, SI. 1983. Separate physiological roles and subcellular compartments for two tetrapyrrole biosynthetic pathways in *Euglena gracilis*. J Biol Chem 258:6799-6807.

Wicke, S, Müller, KF, de Pamphilis, CW, Quandt, D, Wickett, NJ, Zhang, Y, Renner, SS, Schneeweiss, GM. 2013. Mechanisms of functional and physical genome reduction in photosynthetic and nonphotosynthetic parasitic plants of the broomrape family. The Plant Cell 25:3711.

Williamson, DH, Gardner, MJ, Preiser, P, Moore, DJ, Rangachari, K, Wilson, RJM. 1994. The evolutionary origin of the 35 kb circular DNA of *Plasmodium falciparum*: new evidence supports a possible rhodophyte ancestry. Molecular and General Genetics MGG 243:249-252.

Wilson, RJ, Denny, PW, Preiser, PR, Rangachari, K, Roberts, K, Roy, A, Whyte, A, Strath, M, Moore, DJ, Moore, PW, et al. 1996. Complete gene map of the plastid-like DNA of the malaria parasite *Plasmodium falciparum*. J Mol Biol 261:155-172.

Yeh, E, DeRisi, JL. 2011. Chemical rescue of malaria parasites lacking an apicoplast defines organelle

function in blood-stage *Plasmodium falciparum*. PLOS Biol 9:e1001138.

Yoon, EY, Yang, AR, Park, J, Moon, SJ, Jeong, EJ, Rho, JR. 2017. Characterization of a new trioxilin and a sulfoquinovosyl diacylglycerol with anti-inflammatory properties from the dinoflagellate *Oxyrrhis marina*. Mar Drugs 15.

Yoshida, Y, Tomiyama, T, Maruta, T, Tomita, M, Ishikawa, T, Arakawa, K. 2016. De novo assembly and comparative transcriptome analysis of *Euglena gracilis* in response to anaerobic conditions. BMC Genomics 17:182.

Yuzawa, Y, Nishihara, H, Haraguchi, T, Masuda, S, Shimojima, M, Shimoyama, A, Yuasa, H, Okada, N, Ohta, H. 2012. Phylogeny of galactolipid synthase homologs together with their enzymatic analyses revealed a possible origin and divergence time for photosynthetic membrane biogenesis. DNA Res 19:91-102.

Záhonová, K, Füssy, Z, Birčák, E, Novák Vanclová, AMG, Klimeš, V, Vesteg, M, Krajčovič, J, Oborník, M, Eliáš, M. 2018. Peculiar features of the plastids of the colourless alga *Euglena longa* and photosynthetic euglenophytes unveiled by transcriptome analyses. Sci Rep 8:17012.

Záhonová, K, Füssy, Z, Oborník, M, Eliáš, M, Yurchenko, V. 2016. RuBisCO in non-photosynthetic alga *Euglena longa*: divergent features, transcriptomic analysis and regulation of complex formation. PLOS ONE 11:e0158790.

Ziegler, K, Maldener, I, Lockau, W. 1989. 5'-monohydroxyphylloquinone as a component of photosystem I. Zeitschrift für Naturforschung C 44:468-472.

Zimorski, V, Rauch, C, van Hellemond, JJ, Tielens, AGM, Martin, WF. 2017. The mitochondrion of *Euglena gracilis*. In: SD Schwartzbach, S Shigeoka, editors. *Euglena*: Biochemistry, cell and molecular biology. Cham: Springer International Publishing. p. 19-37.